DIPLOMARBEIT

Efficient Elastocaloric Cooling by Cyclic Adiabatic Deformation of Natural Rubber

zur Erlangung des akademischen Grades

Diplom-Ingenieur

im Rahmen des Studiums

Technische Physik

eingereicht von

Florian Greibich

Matrikelnummer 01225210

ausgeführt am Institut für Angewandte Physik
der Fakultät für Physik der Technischen Universität Wien
(in Zusammenarbeit mit Dr. Reinhard Schwödiauer)

Betreuer: Univ. Prof. Dipl.-Ing. Dr. Gerhard Schütz

Wien, 08.02.2019

(Unterschrift Verfasser) (Unterschrift Betreuer)

Abstract

In this diploma thesis I will introduce and examine a new refrigeration system based on the unique thermo-elastic properties of natural rubber. Natural rubber heats up and cools down reversibly during a rapid adiabatic stretch-relaxation cycle. This electrocaloric effect is technically utilized by my specially designed system which exploits the distinctive snap-through instability of a rubber balloon. The heat pump system drives the rubber balloon through a thermodynamic Carnot-like cycle between two heat reservoirs and achieves cooling efficiencies comparable to state-of-the-art refrigerators.

Thus, this diploma thesis demonstrates an alternative pathway towards cooling beyond the state-of-the-art. Optimized systems with improved elastomer materials can work at much higher efficiencies, with low energy consumption and are environmentally friendly.

Acknowledgements

I would like to thank the following persons for their help and support during my thesis:

First and foremost, my gratitude goes to my supervisor, Dr. Reinhard Schwödiauer, my most important source of advice and assistance, whose skills as a researcher and persistence saved the experiment from failure more than once. I stopped counting the hours we spent in the lab, racking our brains over a machine that I had already stopped believing could ever work, until suddenly it did.

I warmly thank my boss, Dr. Martin Kaltenbrunner, for his optimistic and patient support. I also want to thank all my colleagues from the SOMAP group, who always were helpful when needed and made the work place something I always looked forward to go to.

A special thanks goes to Prof. Gerhard Schütz who made this whole thing possible by offering his good name to stand for this thesis.

I also want to thank Prof. Siegfried Bauer, although today, sadly, he is no longer with us. He is the man that inspired me to start researching the topic of this thesis, first through his work, later in person.

Finally, I would especially like to thank my parents for supporting me all those years, for giving me the possibility to study and for not putting any pressure on me to finally finish studying. Without them, I would not be where I am today (literally and figuratively).

Contents

Introduction

Cooling processes are an integral, yet often unnoticed part of everyday life. Applications like food-refrigeration, air-conditioning and a wide variety of industrial processes heavily depend on the use of refrigeration systems. Unsurprisingly, refrigeration systems are one of the world´s main drivers of energy consumption and therefore also a major cause of green-house gas emissions. Air-conditioning alone accounts for 10 % of global electricity consumption [1]. The future demand for air conditioning can be expected to grow dramatically as rising incomes in developing countries enable more and more people to afford such systems for their homes - homes, which are often located in some of the hottest regions on our planet.

Nearly all refrigeration systems currently in use are based on vapor-compression refrigeration. The working principle consists of periodically evaporating and condensing a cooling agent. The most efficient cooling agents unfortunately are highly potent green-house gases. Therefore, leakage from refrigeration systems is suspected to significantly contribute to global warming [1].The application of more climate friendly cooling agents will reduce the already low efficiency even further. A measure for the efficiency is the coefficient of performance (COP). In state-of-the-art refrigeration systems the COP only reaches values of about 3.6 [2]. This means, that an input energy of ca. 278 J is required to remove 1000 J of heat from an object to be cooled.

All this together creates a new dilemma: The increasing demand for refrigeration systems, driven by the rise in global wealth and global temperature, will lead to a soaring electricity demand. That is linked to huge construction costs of new power stations and in addition, poses a serious threat to net stability. Since most of the required electricity will be generated by burning fossil fuels, it further accelerates global warming and hence, cooling demand. In order to break this self-reinforcing cycle and to escape this dilemma of cooling, the development of more efficient and climate-friendly refrigeration systems must be addressed urgently.

In this diploma thesis I will introduce and examine an alternative pathway towards cooling beyond the standard of vapor-compression refrigeration. The goal is to develop a new class of refrigeration systems by taking advantage of the thermal properties of rubber which perhaps might indicate a possible solution of the cooling dilemma. Natural rubber is a material known for centuries. It is cheap, widely available and used for thousands of different purposes in modern-day industry. For products like car tires, damping elements, gaskets and seals, or latex gloves, rubber is the ideal material due to its unique properties of huge elasticity and mechanical robustness. Besides these mechanical properties, rubber also has some fascinating but less well-known thermal properties: Rubber heats up upon stretching and cools down when the stretch is removed. Similarly, when an already stretched rubber is heated, it will contract towards the applied force. These two phenomena were discovered and described first by John Gough in 1805 [3] and further studied by James P. Joule. Both phenomena were summarized as Gough-Joule effect originally, whereas today the term "elastocaloric effect" is commonly used. The elastocaloric effect makes rubber an interesting candidate for the application as a working medium in a thermoelastic heat pump. Thermal imaging of a fully stretched rubber sheet in the shape of an inflated balloon shows a temperature increase of about 10 °C. If the balloon is brought into thermal contact with a heat reservoir, some or all of the temperature related heat can be transferred. After thermal equilibration, when the stretch is removed, the rubber sheet will cool down below the initial temperature. The relaxed rubber sheet can absorb heat from another reservoir with higher temperature, as soon as they establish thermal

contact. Stretching and relaxing a rubber sheet in a way that it alternately contacts two heat reservoirs with different temperatures can thus transport heat between these two reservoirs. According to the theory of an ideal rubber material, the conversion of work into heat upon mechanical stretching is completely reversible. This remarkable circumstance would allow for the rubber-based refrigeration cycle to operate close to Carnot-efficiency [4].

Joule first studied the elastocaloric effect of rubber in 1859 [5]. Since that time, only few attempts have been made to exploit this effect for practical applications. The first known example is a design for a rubber based heat engine introduced by Wiegand [6]. Farris and Lyon conducted preliminary theoretical and experimental studies to assess the feasibility of rubber as a working medium for heat pumps and heat engines [7, 8]. A model developed by Guyomar describes the performance of rubber in a heat pump. The model is based on a prediction of the thermo-elastic behavior of rubber, which was confirmed experimentally [9]. Most scientific work on the topic deals with the concept of rubber based heat engines. Rubber is a suitable elastomer material to turn small temperature differences into useful work. The idea is to take advantage of sources like industrial waste heat that would be lost otherwise [7]. Also several prototypes of elastomer based heat pumps can be found in literature. Gerlach introduced a refrigeration system which operates by uniaxially stretching elongated elastomer strips via a crankshaft [10]. Figure 1.1 shows the design of the device. The elastomer strips are fixed at the ends of the crank and the hinge. As shown on the right side, rotation of the crank results in a periodic stretching and contracting of the elastomer strips. Aluminum plates serve as heat reservoirs. Both are isolated in order to minimize external heat flow. System design allows the elastomer strips to make contact with the upper plate during contraction phase. The lower plate serves as heat sink.

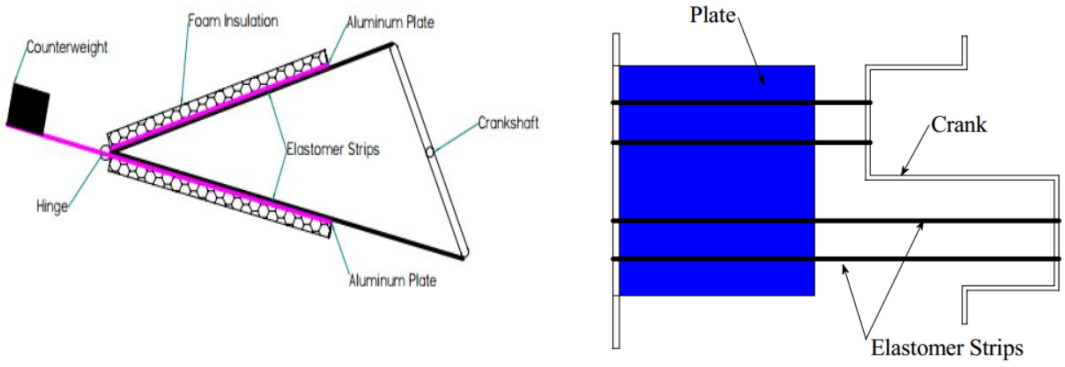

Figure 1.1: *Cooling system with elastomer strips depicted in side view (left) and top view (right) [10].*

Another elegant design proposed by Steinberg is shown in figure 1.2 [11]. A closed-loop rubber band is mounted on two rotating wheels with different diameters. The synchronizing belt imposes the same angular velocity on both wheels. Their different diameters cause diverging strains on the top- and the rear side. The part of the band going towards the broader wheel undergoes a stretch while the other side is contracted. This results in a steady temperature difference which can be exploited by using a suitable heat exchange system.

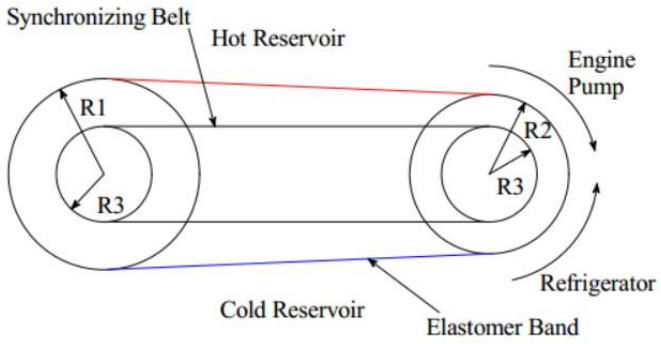

Figure 1.2: *Heat pump system with an elastomer band on two rotating wheels with different diameters [11].*

In 1970 NASA patented the design for a manually operated elastomer heat pump [12]. The usage and operation was considered for the case of a space craft emergency. As shown in figure 1.3, the heat pump consists of two wheels of different size which are arranged eccentrically to each other. The edges of both wheels are connected with several rubber bands. Upon spinning the bigger wheel with the crank, rubber bands will vary in elongation depending on their angular position. The cooling power can be harvested by immersing the short half of the device into a cooling fluid.

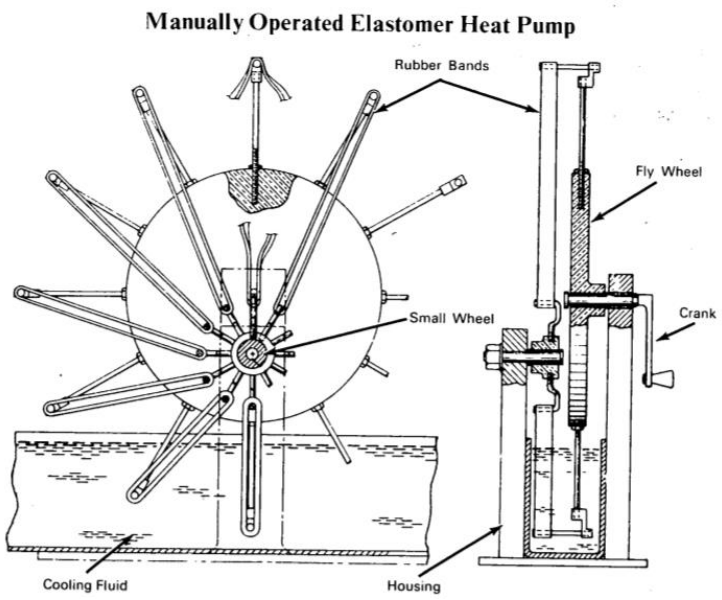

Figure 1.3: *Heat pump design by NASA with rubber bands stretched between two eccentric wheels [12].*

The discussed devices are all based on linear deformation of rubber bands. The first two designs shown were realized as proof-of-concept prototypes by Gerlach and did not achieve the desired result [10]. Frictional losses outweighed the cooling effect and led to an overall warming of the cooling fluid. No report of an experimental realization of the NASA device could be found. However, rubber degradation due to swelling is a commonly known effect and could be a possible source of device failure due to the direct contact of rubber with the cooling fluid.

In this diploma thesis I am proposing a different design for an elastomer refrigeration system which overcomes the problem of frictional heating and fluid related degradation. All parts in my system consist of solid-state materials, where particularly the issue of swelling-induced degradation is

avoided. The main components of the design are schematically depicted in figure 1.4. Its central component is an inflatable elastomer membrane. The inflation is achieved by fixing the membrane to the open side of a pressure vessel with a circular clamp and applying pressurized air from beneath. When the air-pressure exceeds a certain snap-through instability value, the result is a rapid inflation of the elastomer into a balloon with increased temperature. Releasing pressure down to a critical snap-back value leads to an equally swift relaxation of the balloon towards the initial size. The snap instabilities are special properties of balloons made from elastomers with a sufficiently low viscoelasticity. A small change in applied pressure causes a huge and quasi-instant change in balloon volume, making a strong change in strain and consequently a noticeable change in temperature of the membrane.

During operation, the membrane oscillates between two states. In the inflated state the hot elastomer membrane equilibrates with the ambient environment. With a subsequent reduction of the air pressure, the membrane relaxes rapidly into the deflated state and reduces strain and temperature. The cold membrane is in thermal contact with a warmer low temperature heat reservoir (LTR), and the resulting heat-flow from the LTR into the elastomer membrane lowers the temperature in the LTR. A consecutive temperature reduction and refrigeration is maintained with a continuous oscillation of the elastomer membrane between the two states. The continuous operation can be easily achieved by a controlled flow of compressed air with pneumatic valves. I used this method for basic system tests and quick experiments. Though convenient, the compression of air is very energy consuming and thus expensive, and not feasible for efficient operation. As an alternative I developed a Dielectric Elastomer Actuator (DEA) system [13] which allows a more efficient pressure variation for the periodic operation of the elastomer membrane. Details about the experimental systems will be discussed in the chapters three and four.

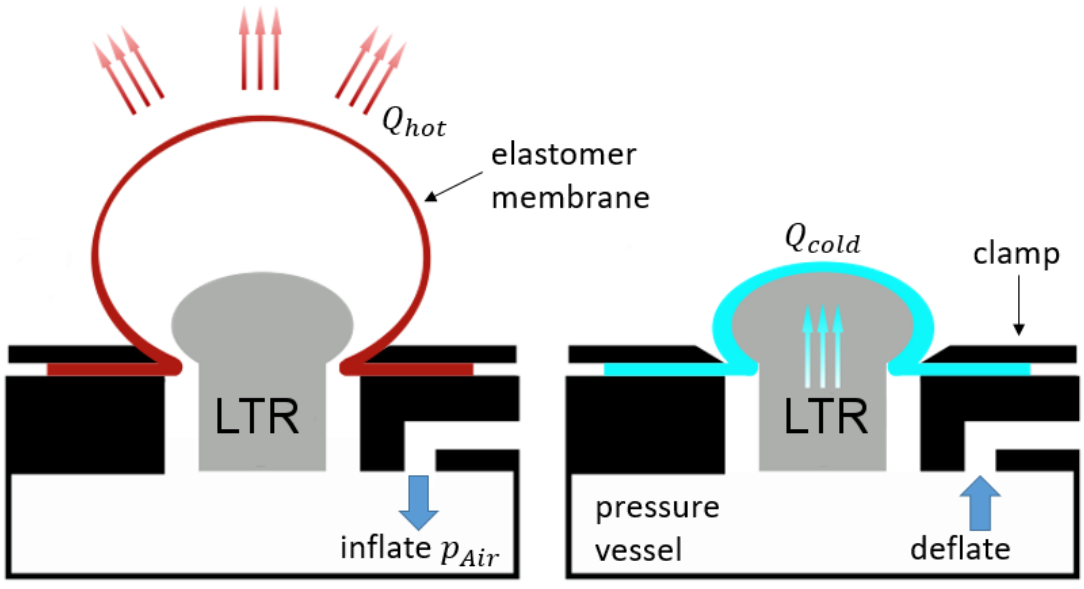

Figure 1.4: *Experimental concept for a refrigeration system operating with inflation (left) and deflation (right) of an elastomer membrane.*

Theory of Operation

This chapter gives a formal, theoretical description of the elastomer refrigeration system. First, a short historical summary of research results introduces the thermo-elastic behavior of rubber. The discussion continues with a condensed review about the thermodynamic properties of elastomer materials, including the elastocaloric effect, and outlines the statistic nature of rubber elasticity. A statistic model is introduced which describes the change in free energy upon rubber deformation. The free energy allows the calculation of the pressure-volume relation for a balloon. The related mechanical instabilities during inflation and relaxation are explained, and the basic requirements for the design of a rubber-based refrigeration system are outlined. Finally, the heat transport of such a system is expressed in detail and the theoretical base for the experimental evaluation of the COP is discussed.

The General Properties of Rubber

Historically, the investigation of the thermo-elastic behavior of rubber started with the experiments performed by Gough. He observed two effects

- Rubber reversibly releases and absorbs heat upon stretching and contracting
- Pre-stretched rubber reversibly contracts and expands upon heating and cooling

Early theories trying to describe rubber elasticity faced great difficulties to grasp this behavior. Especially, since the chemical formula of rubber is identical to that of other hydrocarbons like turpentine, which behaves as a common liquid. This led to the realization that the effects must be caused by a special molecular structure. It was concluded that a material must satisfy three requirements in order to exhibit rubber-like elastic behavior.

- The material consists of long-chain molecules with freely rotating links.
- The secondary forces between these molecules are weak.
- The molecules are connected at a few spots along their length and form a network.

The first requirement was proposed by Meyer [14]. He assumed that increasing temperatures in a long chain molecule cause stronger vibrations of its constituents. The chain-molecules mainly move perpendicular to the chain since restrictive forces are much weaker on the lateral plane than in chain direction. Therefore rising temperatures cause a repulsive force between parallel chains which results in drawing the chain ends together. The equilibrium state is a statistical conformation in which molecular interaction loses directionality. In order to be capable of statistical behavior, the individual chain links need to be able to rotate freely.

The second requirement states that inhibitive intermolecular forces need to be minimal. In fact, these forces in rubber are not different than in a typical liquid. It is because of the third requirement of weak cross-linking that rubber does not actually behave like a liquid. When a few linkages along the length of the molecules are introduced, individual chains can no longer behave independently on a macroscopic scale. However, the low number of linkages ensures enough remaining local freedom for statistical fluctuations to happen. The statistic fluctuations of a chain network are affected by a strong macroscopic deformation of the rubber material. Thus, a strong deformation also affects the entropy of such a system, and a related temperature change can be explained with basic concepts of thermodynamics.

Thermodynamics

The thermodynamic treatment of rubber elasticity given below refers to all rubber-like materials in general. The theory does not distinguish between different chemical compositions, since it is based on universal statistical and thermodynamic considerations.

A qualitative understanding of the thermo-mechanical behavior is reached by establishing a general thermodynamic theory. Quantitative predictions, however, require a more refined model, taking into account the molecular structure of the material [15].

The first law of thermodynamics describes the change in internal energy, dU, due to a change in heat, dQ, and work, dW, that is performed by or on the system.

$$dU = dQ + dW \tag{1}$$

The thermodynamic system under consideration is a loosely crosslinked polymer network (rubber elastomer) and the internal energy is related to the bond lengths and the bond angles between the monomers of a polymer chain. In the relaxed state the polymer chains are statistically folded and intertwined into each other. An applied stretching force will gradually change their conformation in a direction parallel to the applied force.

Any moderate stretch deformation of a rubber elastomer causes a spatial rearrangement of the polymer chains, whereas the related changes of both the bond lengths and the bond angles between the chain monomers remain reasonably small. This is especially true for rubber networks with freely rotating bonds between the monomers, since these facilitate the conformational changes of the polymer chains. For such networks the change of internal energy can be neglected. This has been demonstrated experimentally by several authors [16, 17]. Because of this result, $dU = 0$, the heat of the system can be directly related to the work which is performed by a tensile force, f, against the rubber network that stretches by the length dl

$$dQ = -dW = -f dl \tag{2}$$

The change in heat corresponds to a change in entropy according to the second law of thermodynamics

$$dQ = T dS \tag{3}$$

By inserting Eq. (3) into Eq. (2) the tensile force can be related to the entropy gradient, yielding the governing equation for entropy-elasticity

$$f = -T\left(\frac{\partial S}{\partial l}\right)_T \tag{4}$$

In order to find an expression for the stretch-dependent change in temperature, the correlated change in heat needs to be expressed by

$$dQ = c_l dT \tag{5}$$

where c_l denotes the heat capacity of the unstrained rubber network.

By inserting Eq. (4) and Eq. (5) into Eq. (2) and integrating on both sides, the temperature difference caused by deformation of the system can eventually be written as

$$\Delta T = -\frac{T}{c_l}\int_{l_0}^{l}\left(\frac{\partial S}{\partial l}\right)_T dl \tag{6}$$

Eq. (6) shows that the change in temperature is governed by the entropy gradient. Hence, ΔT is determined by the entropy function of the material. Figure 2.1 shows a schematic graph of an entropy function and its gradient. The maximum of the entropy defines the equilibrium length l_0. According to Eq. (4) the tensile force at this point is zero. When the length is increased beyond l_0 the entropy gradient becomes negative. Due to the negative sign in Eq. (6), the result is a positive temperature change.

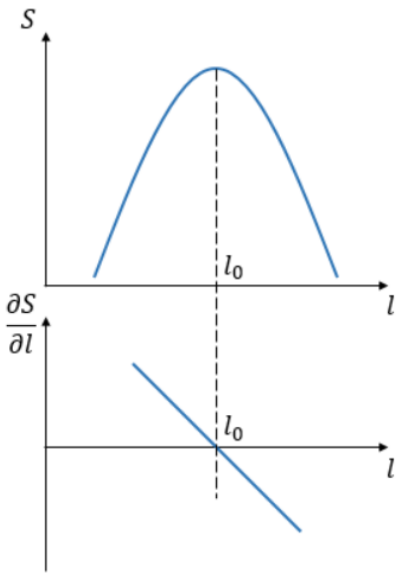

Figure 2.1: *Example for an entropy function and its corresponding gradient.*

Entropy and Energy of Deformation

The entropy of a long polymer chain is described by the Boltzmann equation, $S = k_B ln(P)$, where k_B is the Boltzmann constant, and P represents the probability distribution for the conformation of a polymer chain with rotatable bonds. Depending on the specific conformation, the polymer chain has a given end-to-end length, l, and is described by the probability distribution

$$P(n,l) = \left(\frac{b(n)}{\sqrt{\pi}}\right)^3 e^{-b(n)^2 l^2} \tag{7}$$

where $b = \frac{3}{2na^2}$, and n denotes the number of single chain segments, each having a length a. This Gaussian probability distribution has been derived and investigated by a number of authors in the first half of the 20th century [15, 18-21]. With Eq. (7) the entropy of an undisturbed chain with an equilibrium end-to-end length of $l_0 = \sqrt{x_0^2 + y_0^2 + z_0^2}$, results in

$$s_0 = c - k_B b^2 l_0^2 \tag{8}$$

where c is an arbitrary constant. A deformation of the polymer chain in the x-, y- and/or z-direction is described with respective strain factors

$$\lambda_1 := \frac{x}{x_0},\ \lambda_2 := \frac{y}{y_0},\ \lambda_3 := \frac{z}{z_0} \tag{9}$$

and the entropy change related to such a deformation is expressed by

$$\Delta s = s - s_0 = -k_B b^2\{(\lambda_1^2 - 1)x_0^2 + (\lambda_2^2 - 1)y_0^2 + (\lambda_3^2 - 1)z_0^2\} \tag{10}$$

The total entropy change for a piece of rubber with N chains per unit volume is obtained by summation

$$\Delta S = \sum_i^N \Delta s_i = -k_B b^2 \left\{(\lambda_1^2 - 1)\sum_i^N x_{0,i}^2 + (\lambda_2^2 - 1)\sum_i^N y_{0,i}^2 + (\lambda_3^2 - 1)\sum_i^N z_{0,i}^2\right\} \tag{11}$$

Since the directions of the chain vectors $\overrightarrow{r_0} = (x_0, y_0, z_0)$ in the unstrained state are completely random, we can write

$$\sum x_{0,i}^2 = \sum y_{0,i}^2 = \sum z_{0,i}^2 = \frac{1}{3}\sum r_{0,i}^2 \tag{12}$$

And

$$\sum r_0^2 = N\bar{r}_0^2 \tag{13}$$

where $\bar{r}_0$ is the mean square length of a single chain in the unstrained state. One can substitute $\bar{r}_0$ with the corresponding value for a free chain, given by $\bar{r}_0^2 = 3/2\, b^2$. This yields the final result for the entropy change upon deformation

$$\Delta S = -\frac{1}{2}Nk_B(\lambda_1^2 + \lambda_2^2 + \lambda_3^2 - 3) \tag{14}$$

Finally, the Helmholtz Free Energy of a network consisting of *N* polymer chains is given by the familiar relation $W = -T\Delta S$. With the definition of the strain invariant, $J = \lambda_1^2 + \lambda_2^2 + \lambda_3^2 - 3$, the energy can be expressed concisely by

$$W = \frac{1}{2}NkTJ \tag{15}$$

Snap-Through Instability

A pressurized balloon of natural rubber shows a notable snap-through instability with a sudden change in volume as the internal gas pressure reaches a critical value. This instability results from a strongly non-linear pressure-volume relation which can be derived from the Helmholtz Free Energy given with Eq. (15). The strain factors are determined by the basic requirement $\lambda_1\lambda_2\lambda_3 = 1$, which accounts for the incompressibility of the rubber material. As a consequence, the strain can be expressed by the size of the balloon with the initial unstrained radius r_0, and the strained radius r.

$$\lambda_1 = \lambda_2 = \frac{r}{r_0} \tag{16}$$

$$\lambda_3 = \frac{1}{\lambda_1\lambda_2} = \frac{r_0^2}{r^2} \tag{17}$$

Using the radial strain factor $\lambda = r/r_0$, equation (15) calculates to

$$W = \frac{1}{2} N k_B T (2\lambda^2 + \lambda^{-4} - 3) \tag{18}$$

The tensile force on the balloon membrane is obtained by

$$f = \frac{dW}{dr} = 2N k_B T \frac{1}{r_0} (\lambda + \lambda^5) \tag{19}$$

And the internal gas pressure on the surface area, $A = 4\pi r^2$ of the balloon is

$$p(r) = \frac{f}{A} = N k_B T \frac{1}{2\pi\, r_0^3} (\lambda^{-1} + \lambda^7) \tag{20}$$

The diagram in figure 2.2 shows the gas pressure according to Eq. (20). At the beginning of inflation a small increase in volume requires a large increase in pressure until the maximum value p_{max} is reached. This point marks the snap-through instability from where on the balloon continues to grow in size. The only stable state beyond the snap-through instability is reached, if the balloon grows to infinite size, with $\lambda \to \infty$, where the internal pressure drops to $p = 0$. This unreasonable result requires an unrealistic rubber material with polymer chains of infinite length. A more realistic description has been proposed by Gent [22]. He assumed a maximum value for the strain invariant at which the strained rubber reaches a limiting state as the polymer chains become fully stretched to their finite length. Such behavior can be simulated with an empirical modification of the Helmholtz free energy function

$$W = \frac{E}{6} J_m \, ln(1 - J/J_m) \tag{21}$$

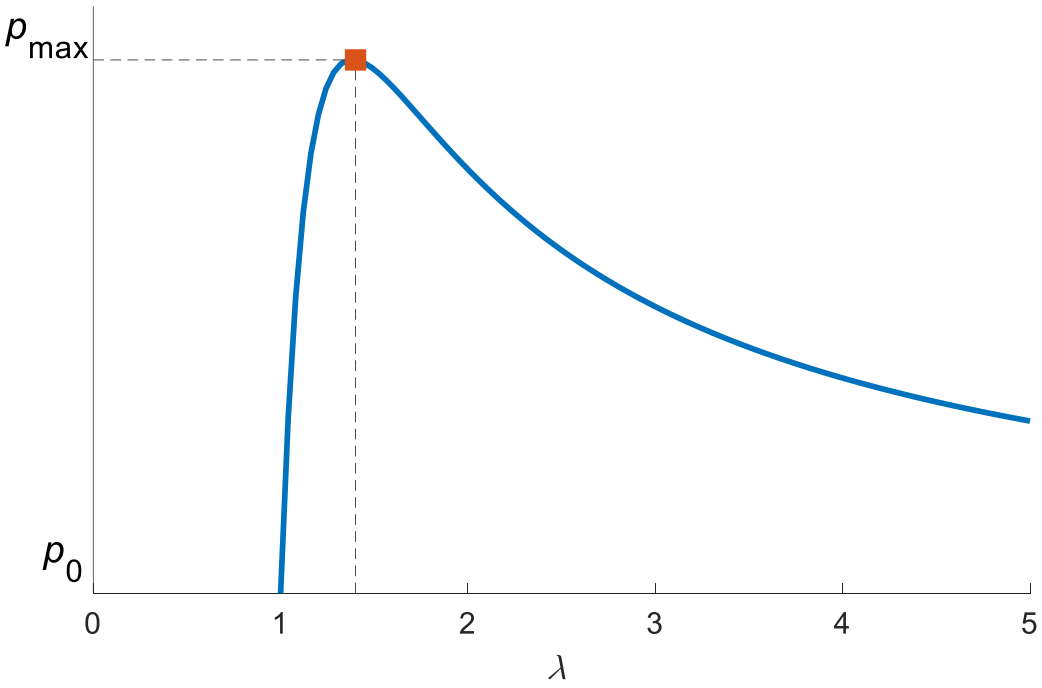

Figure 2.2: *Pressure versus strain factor of a balloon according to Eq. (20).*

where J_m denotes the maximum value for J, the strain invariant, and E expresses the small-strain tensile modulus of the material. This energy function can be used to calculate the pressure that is required to inflate a thin, plain circular sheet of rubber material with initial thickness h and a radius a to a size of λa. The result has been given by [23, 24]:

$$p = \frac{4h}{a\lambda}\left(1 - \frac{1}{\lambda^6}\right)\frac{dW}{dJ} \tag{22}$$

With the conditions of Eq. (16) and (17) for the inflation of a balloon, the related pressure can be plotted as a function of the radial strain factor λ. The diagram in figure 2.3 shows this function. The pressure maximum, p_{max}, occurs at a strain of $\lambda = 7^{1/6}$. This maximum is identical with the maximum of the pressure function given in Eq. (20). Thus, for small strains with pressure values below p_{max} both pressure functions, Eq. (20) and Eq. (22), show practically identical behavior. With larger strains beyond λ=$7^{1/6}$ the pressure function drops to a minimum (dashed line) and eventually rises towards infinity as the strain approaches the maximum value. The inflation of a balloon from the initial state I, with a pressure of p_0, up to the unstable state II at p_{max}, is followed by a rapid snap-through expansion from state II to III, if the pressure is maintained constant with a sufficiently large pressure reservoir. A subsequent pressure decrease causes a stable decrease in size towards the unstable state IV which is followed by a rapid snap-back to state V. The swift size transitions from state II to III and from IV to V are closely linked with an adiabatic temperature change as discussed previously. The temperature increases upon rapid expansion from II to III. With the rapid contraction from state IV to V the temperature reversibly decreases. If the rubber membrane is driven through a full cycle with oscillating pressure between p_0 and $p_{\max}$, the transport of thermal energy between two temperature reservoirs can be achieved. Such a heat transport system requires two temperature reservoirs which are thermally contacted by the relaxed and strained rubber balloon at state I and III respectively.

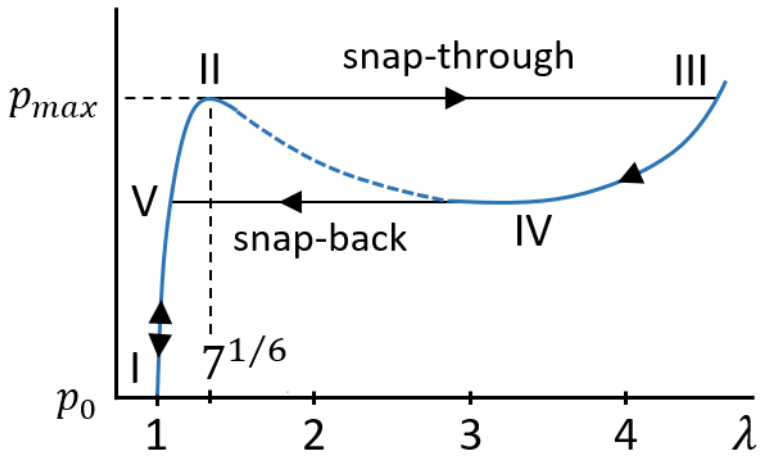

Figure 2.3: *Pressure versus strain factor of a balloon*

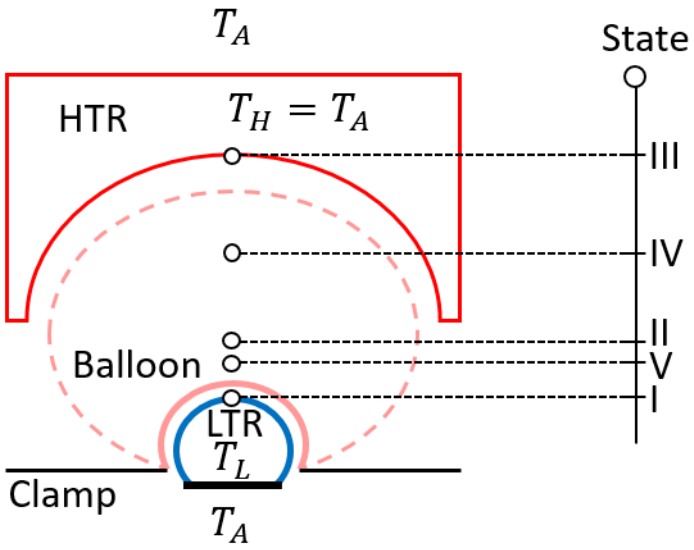

Figure 2.4: *Schematic illustration of a heat transport system with a rubber balloon oscillating between a low temperature heat reservoir at state I and a high temperature heat reservoir at state III.*

Heat Transport and Reservoir Cooling

The diagram in figure 2.4 schematically shows a heat transport system that is composed of a high temperature heat reservoir (HTR), a low temperature heat reservoir (LTR) and a rubber balloon fixed by a circular clamp. The temperatures of the heat reservoirs and the rubber balloon are T_H, T_L, and T_R respectively. The convex shape of the LTR follows the shape of the relaxed balloon at state I, and the concave shape of the HTR follows the shape of the maximally inflated balloon at state III. The HTR is supposed to be in thermal equilibrium with the ambient environment. The temperature of the environment is T_A, and the temperature of the HTR is thus $T_H = T_A = const.$ As the balloon inflates up to the unstable state II, its size increases rapidly to state III and the rubber material heats up. The excess heat of the inflated balloon is transferred to the HTR by thermal contact and the temperature of the inflated rubber balloon adjusts to T_A. As the size of the balloon decreases to state IV the rapid snap-back to state V reduces the temperature by a value of ΔT according to Eq. (6). The subsequent relaxation to state I brings the cold rubber balloon in thermal contact with the warmer LTR and this difference in temperature drives an internal heat flux from the LTR to the rubber. The heat flux continues until both elements have reached equilibrium at a mean temperature, T_M. This mean temperature is determined by energy conservation which is expressed by the heat balance equation

$$m_L c_L T_L + m_R c_R T_R = m_L c_L T_M + m_R c_R T_M \tag{23}$$

with the mass m_L and the specific heat c_L of the LTR, and the mass m_R and the specific heat c_R of the rubber membrane. The mean temperature in thermal equilibrium thus is

$$T_M = \frac{m_L c_L T_L + m_R c_R T_R}{m_L c_L + m_R c_R} \tag{24}$$

Consequently, the temperature of the LTR has dropped by a value of $\Delta T_L = T_L - T_M$ and the heat

transported away from the LTR is

$$\Delta Q_L = m_L c_L \Delta T_L \tag{25}$$

With every actuation cycle of the rubber balloon the temperature of the LTR drops further and because of the variable reservoir temperature, T_L, Eq. (24) serves as a function, $T_M(T_L)$, for the next actuation cycle: The initial T_L becomes $T_{M,1} = T_M(T_L)$ after the first cycle and $T_{M,2} = T_M(T_{M,1})$ after the second cycle, and so on. The explicit form of this iterative sequence as well as the convergent temperature can be expressed in a concise algebraic notation with the introduction of two caloric quantities

$$\mu_L = \frac{m_L c_L}{m_L c_L + m_R c_R}, \mu_R = \frac{m_R c_R}{m_L c_L + m_R c_R}$$

With these quantities Eq. (24) is converted to

$$T_M(T_L) = \mu_L T_L + \mu_R T_R = \mu_L T_L + (1 - \mu_L) T_R \tag{26}$$

The iterative application of Eq. (26), arranged in a table for n actuation cycles, results in

$$\begin{array}{lll} n{=}0{:} & T_{L,0} = & T_A \\ n{=}1{:} & T_{L,1} = & T_M(T_{L,0}) = T_R + (T_A - T_R)\mu_L \\ n{=}2{:} & T_{L,2} = & T_M(T_{L,1}) = T_R + (T_A - T_R)\mu_L^2 \\ \vdots & \vdots & \\ n{:} & T_{L,n} = & T_M(T_{L,n-1}) = T_R + (T_A - T_R)\mu_L^n \end{array}$$

The table reveals the explicit form of the temperature sequence. With the pre-equilibrium temperature of the rubber membrane in state I, $T_R = T_A - \Delta T$, the sequence takes the form

$$T_{L,n} = T_A - \Delta T + \Delta T \mu_L^n \tag{27}$$

and describes the temperature evolution of the LTR for every single actuation cycle. The initial temperature is $T_{L,0} = T_A$, and every cycle reduces the temperature by $(1 - \mu_L^n)\Delta T$. Because of $\mu_L < 1$ the temperature reduction is growing smaller by every cycle. In the limit of $n \to \infty$ cycles the convergent temperature is

$$T_{L,\infty} = T_A - \Delta T \tag{28}$$

Therefore, the minimum temperature of the LTR is limited by the entropic temperature drop and the minimum temperature of the relaxed rubber membrane.

The temperature sequence of Eq. (27) can be expressed in terms of discrete time steps with $t_n = n\tau$, where τ denotes the temporal period of a full actuation cycle. In addition, the substitution $\gamma = -ln(\mu_L)$ transforms the temperature sequence into

$$T_L(t_n) = T_A - \Delta T + \Delta T e^{-\gamma \frac{t_n}{\tau}} \tag{29}$$

A graphical representation of this equation, both as discrete sequence and as a continuous function, is shown by the diagram in figure 2.5. The large dots indicate the discrete equilibrium temperatures of the LTR at the end of each actuation cycle, the dashed line is the continuous exponential function which describes the overall temperature decrease versus time. The step-like continuous line between the equilibrium temperatures suggests an unrealistic instant temperature drop of the LTR at the end of every actuation cycle. A more realistic description of the time for temperature equilibration between the LTR and the rubber membrane requires the solution of the heat equation

$$\frac{dT}{dt} - D\frac{d^2T}{dz^2} = 0 \tag{30}$$

Eq. (30) describes the temperature function $T(z, t)$ of an element with the thermal diffusion coefficient, $D = k/(\rho c)$. Carslaw and Jaeger [25] present the general solution by

$$T(z,t) = T_1 + T_2\, erf\left(\frac{z}{2\sqrt{Dt}}\right) \tag{31}$$

for a composite solid where the flat surfaces of two materials with different temperatures are brought into thermal contact. The two constants, T_1, and T_2, need to satisfy the initial and the boundary conditions of the system.
The spatial and temporal behavior of temperature is determined by the error function, $erf(x)$, which converges to the value 1. This convergence limit is practically reached for all $arguments \leq 2$. The argument of the temperature function thus suggests that a surface layer of thickness *z*

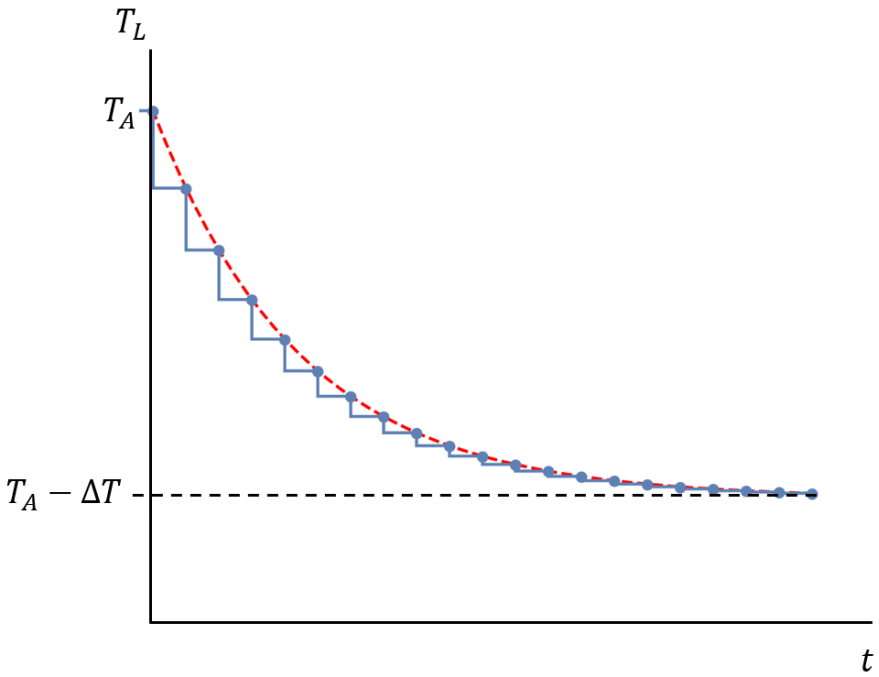

Figure 2.5: *Step-like temperature drop of the LTR (continuous blue), and the related exponential decrease (dashed red) vs. cooling time.*

reaches thermal equilibrium after the time

$$t_e = \frac{z^2}{16D} = \frac{1}{16}\frac{\rho c}{k} z^2 \tag{32}$$

The largest value of t_e for either the LTR, the HTR, or the rubber membrane, defines the lower limit for the duration of an actuation cycle.

Coefficient of Performance

Each actuation cycle requires an input energy for the cyclic operation of the rubber balloon. The energy per cycle is equivalent to a pressure–volume work of

$$W_R = \oint p \, dV, \tag{33}$$

The actuated rubber removes a discrete amount of heat, ΔQ_L , from the LTR. The related efficiency is described by the coefficient of performance (COP) defined by

$$\epsilon = \frac{\Delta Q_L}{W_R} \tag{34}$$

This parameter quantifies the effectiveness of a refrigeration system and can be used for comparison between different systems. However, a strict comparison is valid only, if all significant thermodynamic factors, especially the temperature of the LTRs, are equal. Since the temperature $T_{L,n}$ of a finite LTR decreases with a growing number of actuation cycles, the temperature relevant for the calculation of ϵ is the initial temperature, $T_{L,0}$, since the first actuation cycle removes the maximum heat

$$\Delta Q_{L,0} = \frac{m_L c_L m_R c_R}{m_L c_L + m_R c_R}[T_{L,0} - (T_A - \Delta T)] \tag{35}$$

from the LTR. In general, the initial temperature is identical with the ambient temperature, $T_{L,0} = T_A$, and in this case the maximum COP is expressed by

$$\epsilon_{max} = \frac{1}{W_R}\frac{m_L c_L m_R c_R}{m_L c_L + m_R c_R}\Delta T = \frac{\Delta T}{W_R}(m_L c_L || m_R c_R) \tag{36}$$

According to this formula, the improvement of ϵ_{max} towards larger values requires the optimization of the temperature-work relation, $\Delta T/W_R$, and the adjustment of the LTR to the caloric properties of the rubber membrane, described by $m_L c_L || m_R c_R$. This factor of the form $xy/(x+y)$ increases with the increase of either parameter and reaches a maximum value for $m_L c_L = m_R c_R$. For such a system the temperature drop of the LTR is $\Delta T_L = T_{L,0} - T_{M,1} = \Delta T/2$ and the removed heat, $\Delta Q_{L,0} = m_L c_L \, \Delta T/2$, is maximized. Considerably more complicated to describe is the ideal temperature-work relation. The adiabatic temperature change, ΔT, depends on the change in entropy upon deformation, $(\partial S \,/\, \partial \lambda)$, and this quantity is strongly connected to microscopic parameters of the rubber material (molecular weight, number of cross-links, tendency of crystallization upon elongation, etc...). Therefore, the optimization of $\Delta T/W_R$ remains very much an experimental exercise.

Experimental Setup

The experiments are performed with two different setups. The first setup serves to determine the cooling capacity of the elastomer membrane. Compressed air is used as actuating agent. Figure 3.1 shows a schematic illustration.

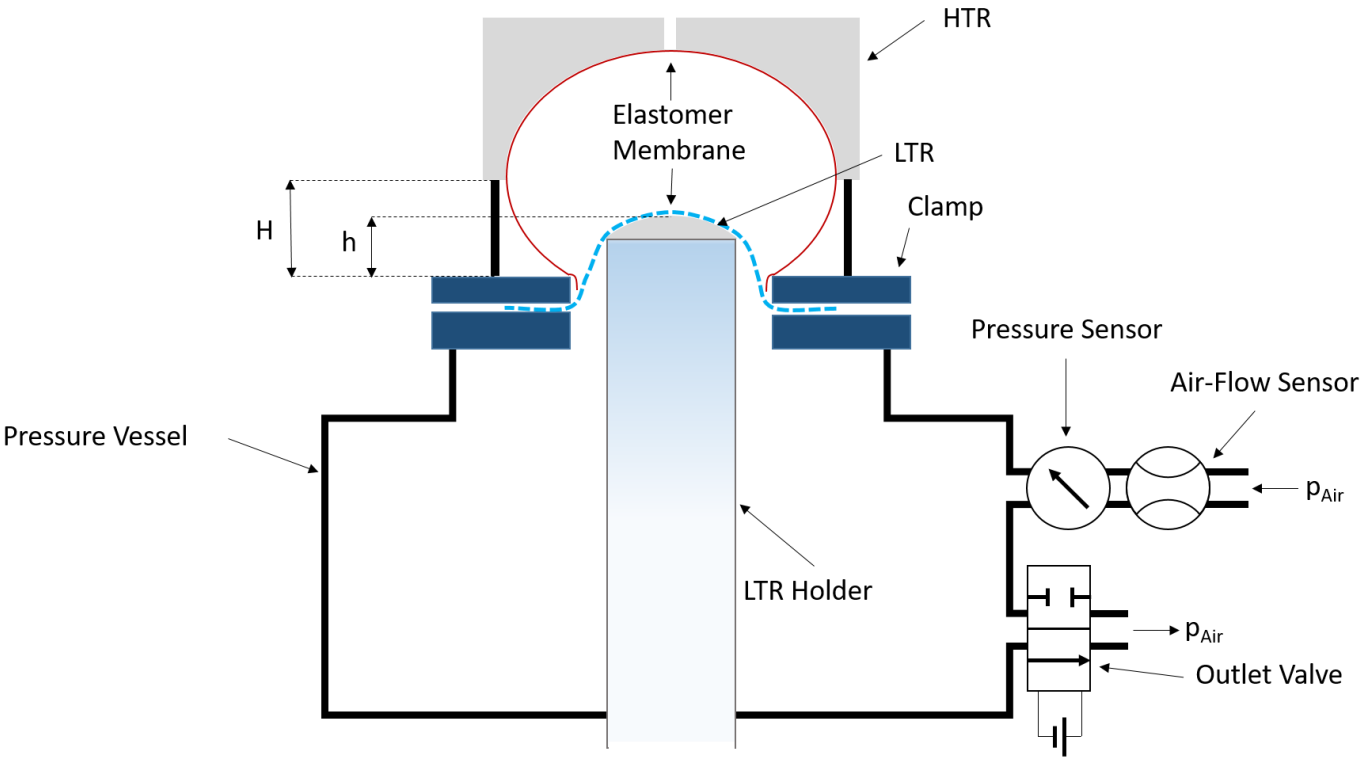

Figure 3.1: *Setup 1 with externally triggered outlet valve.*

The pressure vessel is a polypropylen tube (Ostendorf Kunsttoffe GmbH, Vechta, Germany) with a length of 480 mm and a diameter of 105 mm. The pressurized air is supplied through a pneumatic tubing with an inner diameter of 4 mm. The vessel has an air inlet, which remains opened continuously and an outlet, which can be opened and closed by an externally triggered Festo VACS-H1P-A1-1 valve (Festo, Esslingen am Neckar, Germany). An SFAB-50U-HQ8 air flow sensor (Festo, Esslingen am Neckar, Germany) measures the flow rate entering the tube and a Jumo dTrans p30 pressure sensor (JUMO, Fulda, Germany) monitors the pressure within the vessel. The clamp for fixation of the elastomer membrane is mounted on top of the pressure vessel. It consists of two nylon disks which can be fixed on each other with screws and can be varied in aperture. Above the clamp, concentric to the aperture, a HTR is mounted at a height H = 13 mm. The cylinder has an outer diameter of 80 mm and a height of 34 mm. On its rear side there is an indentation shaped like a semi-ellipsoid with a diameter of 65 mm and a depth of 35 mm. A small hole was drilled in the center of the top side in order to allow the air to escape when the elastomer membrane is inflated. Below the elastomer membrane, the LTR is placed at a height h = 10 mm, mounted on top of the LTR holder. In figure 3.4 a detailed illustration of the LTR holder is given. In figure 3.5 the clamps are shown. All measured data is digitalized with a BNC 2110 DAQ chip (National Instruments, Austin, USA).

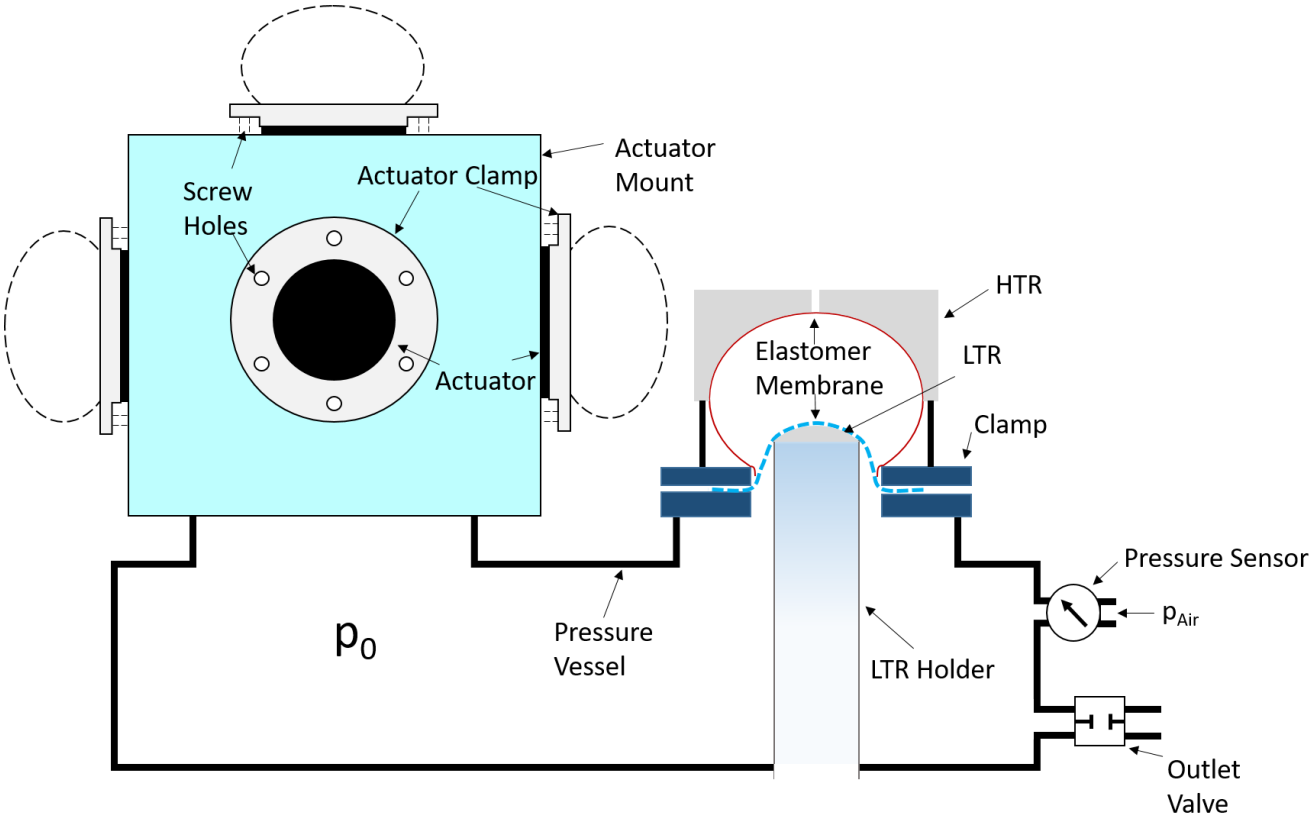

Figure 3.2: *Setup 2 with DEA pressure supply.*

In Setup 2, schematically illustrated in figure 3.2, the outlet valve is permanently closed and the pressure vessel is filled with air at a base pressure of 55-75 mbar. The pressure difference necessary to inflate the elastomer membranes is delivered by DEAs. Up to five DEAs are supported by a cuboid actuator mount connected to setup 1, with inner dimensions of 120x120x130 mm^3. It is made up of Plexiglas with a thickness of 15 mm. The circular apertures for the DEAs measure 45 mm in diameter. The DEAs are fixed on the mount with clamps similar to those used for the elastomer membrane. In figure 3.5 a detailed model of the clamps is shown. Two types of elastomer membranes were used, OPPO Band[1] (OPPO MEDICAL, Seattle, USA) and SANCT Band[2] (Wagus GmbH, Rheinstetten, Germany). Samples were produced by cutting circular sheets with a diameter of 49 mm. Table 3.1 gives an overview over the samples used in the experiments and their properties.

Table 3.1: *Sample brands and properties*

Sample Name	Brand Name	Thickness (µm)	Mass (g)	Density (g/cm^3)
Sample 1	OPPO grey	450	0.85	1
Sample 2	SANCT grey	420	0.8	1
Sample 3	SANCT orange	180	0.34	1
Sample 4	SANCT pink	140	0.25	1

[1] Supplier: http://antarmedizin.de/
[2] Supplier: https://www.wagus.de/

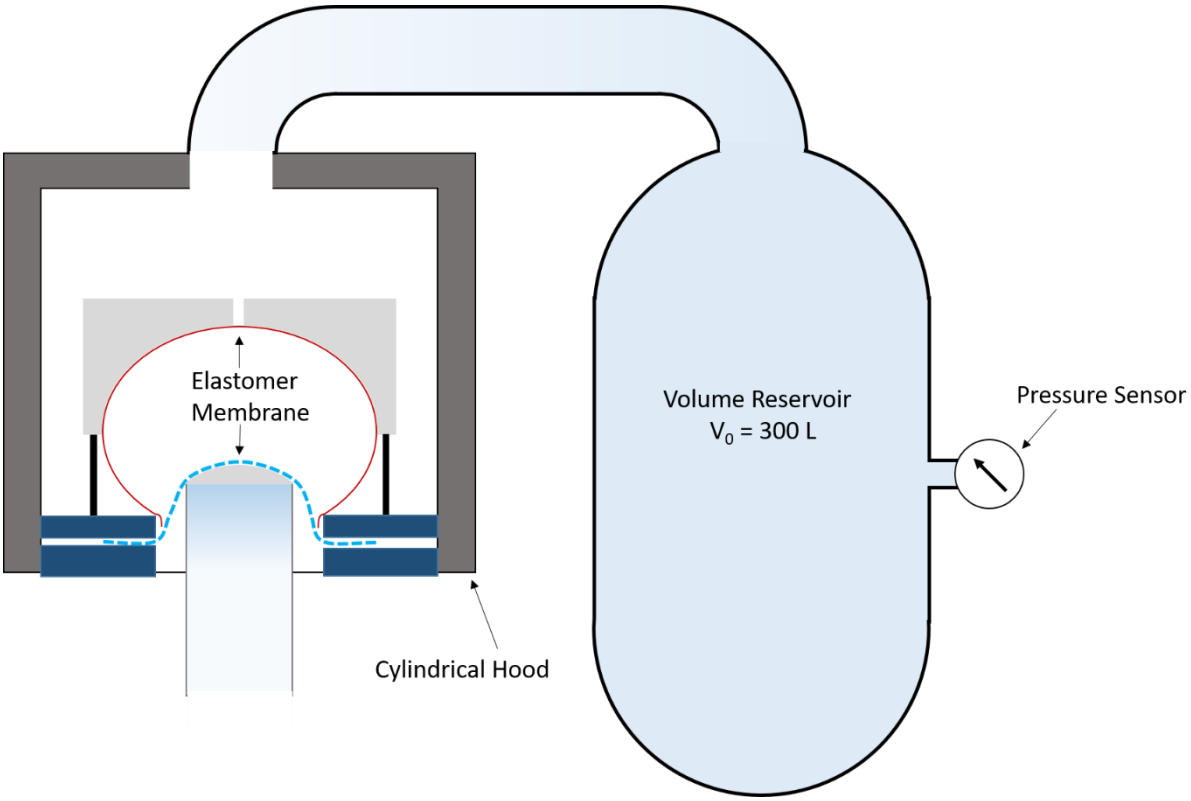

Figure 3.3: *Setup used to measure the balloon volume*

In order to compute the p-V-diagram of an actuation cycle, the balloon volume is measured over time. As shown in figure 3.3 the top side of the LTR is coupled to a large volume reservoir of 0.3 m^3. The aperture of the cylindrical hood encloses the clamp in an airtight fashion. The hood is connected to the reservoir by a hose with a length of 5 m and an inner diameter of 40 mm. A Jumo dTrans p30 (JUMO, Fulda, Germany) pressure sensor is attached to the reservoir.

Since the volume change ΔV takes place in a very rapid manner, the associated thermodynamic change of state can be assumed to be adiabatic. Therefore ΔV can be computed from the pressure data by using

$$p_0 V_0^{\kappa} = p_1(t) V_1(t)^{\kappa} = p_1(t)\big(V_0 - \Delta V(t)\big)^{\kappa} \Rightarrow \Delta V(t) = V_0 \left[1 - \left(\frac{p_0}{p_1(t)}\right)^{\kappa}\right]$$

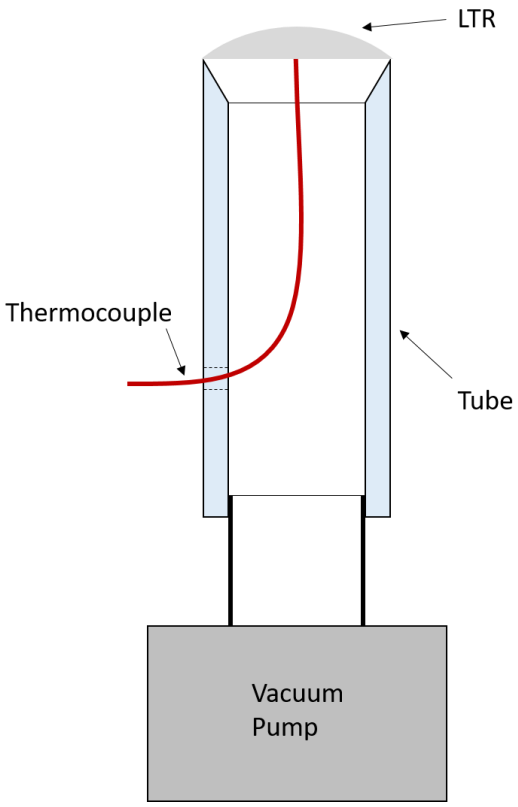

Figure 3.4: *Schematic drawing of the LTR holder.*

The LTR holder, as shown in figure 3.4, consists of a 250 mm long polypropylen tube with an outer diameter of 20 mm and a wall thickness of 3.5 mm. The LTR consists of aluminum and is shaped like a spherical segment with a diameter of 17.5 mm and a height of 3.25 mm. It is attached to the top side of the tube with epoxy resin. In order to minimize parasitic heat flow from the tube on the LTR, the area of contact is reduced by sloping the tube-wall towards the inside. The rear side of the tube is connected to a vacuum pump. The temperature in the LTR is measured with a type-K thermocouple which is attached on the central rear side of the LTR. The thermocouple exits the LTR holder through a small hole which is sealed with silicon glue.

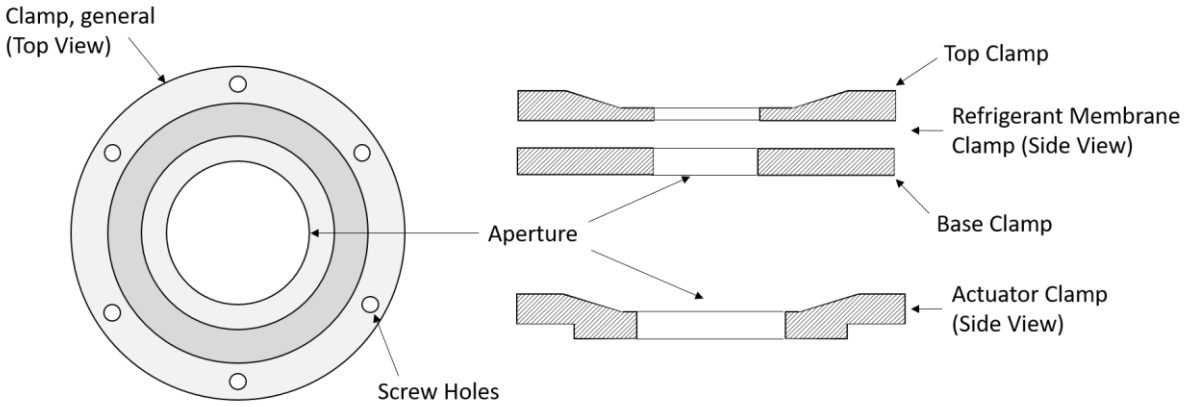

Figure 3.5: *Schematic drawing of the elastomer membrane and the actuator clamps in top view (left) and side view (right).*

Figure 3.5 shows the clamp for the elastomer membrane. It consists of two nylon discs which both have an outer diameter of 100 mm. The lower base clamp is a flat disc with a thickness of 10 mm and an inner diameter of 30 mm. The top clamp has a thickness of 8 mm at its outer region and then gradually thins to an inner region with a thickness of 2 mm and a diameter of 45 mm. The top clamp was built in three different versions with apertures of 30 mm, 35 mm and 40 mm. The thinning towards the center allows the elastomer membrane to inflate without encountering any edges.

The actuator clamps were 3D-printed with ABS. They have an outer diameter of 90 mm, a total thickness of 6 mm and an aperture of 45 mm. Again, on the top side the clamp thins down to the center to a height of 2 mm. The inner region has a diameter of 56 mm. On the rear side an offset bottom with a diameter of 70 mm and a thickness of 2 mm was implemented.

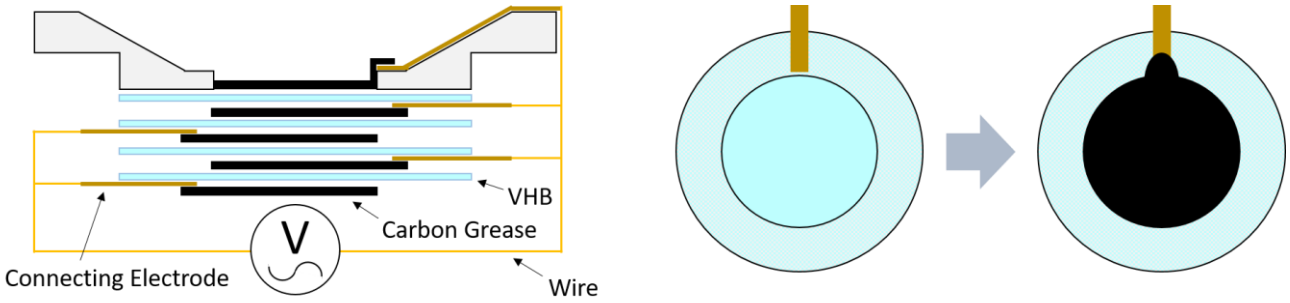

Figure 3.6: *The structure of a multilayer DEA stack (left). The positioning of the connecting electrodes and the application of carbon grease (right).*

The DEA consists of a layered stack of VHB 4905-F (3M, Saint Paul, USA) and carbon grease (see recipe below), shown on the left side of figure 3.6. The number of VHB layers depends on the stress-strain properties of the elastomer membrane in the refrigeration system. The moduli of the elastomer membrane and of the actuator stack need to match so that both can interact. For one layer, two pieces of the 0.5 mm thick VHB tape are stuck together in order to obtain a 1 mm thick layer. It was observed that by connecting two thinner pieces, the dielectric strength of the layer could be significantly enhanced compared to 1 mm VHB tape. Prior to the assembly of the DEA, the self-created 1 mm VHB layer is biaxially pre-stretched with factor of 1.8 (areal stretch 1.8 x 1.8). The pre-stretched tape is firmly pressed against the rear side of the actuator clamp, where it sticks due to its self-adhesive properties. A 0.1 mm thin and 2 mm wide copper tape is attached onto the membrane within the area of the bottom ring. The strip is placed close before the aperture in order to avoid any perforation by sharp edges. A thin layer of carbon grease is placed on both sides of the membrane and also makes contact with the near end of the copper strip (figure 3.6b).

The DEA consists of an arbitrary number of such layers stacked on top of each other. The copper strips are attached on opposing sides in an alternating manner. The uppermost strip is attached to the top side of the clamp. All strips of one side are connected to the same pole of the voltage source. This ensures that every layer of VHB is subject to an electric field. In this thesis three- and four-layered actuators where used.

For the carbon grease, Black Pearls 2000 Carbon Black (CABOT, Boston, USA) is mixed with Elbesil 50 silicon oil (Quax GmbH, Otzberg, Germany) in a weight ratio of 1:15. The mixture is blended in a speed-mixer for 10 min at 2000 rpm with 5 steel balls added and another 20 minutes at the same speed without steel balls. Blending is interrupted in ten minute intervals to allow the mixture to cool down. The result is a smooth, creamy carbon paste easy to spread on elastomeric surfaces.

Results and Discussion

At the beginning of this experimental work, a number of test measurements were carried out to identify the optimum settings of the experiment. A number of parameters were examined for their impact on device performance, including the aperture of the clamp, the height of the LTR and the frequency of the actuation cycle. Different types of elastomer membranes with varying membrane thicknesses were investigated in order to test cooling performance and lifetime. In every experiment the temperature curve over time was determined. To analyze the data, the curve was fitted with an asymptotic exponential model. The fit yields two key values that serve to evaluate device performance, the maximum temperature drop and the decay constant as a measure of power. All results are displayed in a plot with these key values as axes.

Preliminary Experiments

Figure 4.1 shows a typical temperature-time curve with its corresponding fit, the exponential law indicated in the graph. The maximum temperature difference and the decay constant of the exponential law are the key parameters necessary to assess the performance of the cooling process. The decay constant is needed to compute the COP of the process, while the maximum temperature difference determines the relative COP (fraction of Carnot efficiency). The performance of all further experiments is displayed in a plot with the decay constant on the abscissa and the maximum temperature difference on the ordinate. However, it is important to note that this representation is chosen for mere convenience, there is no functional relation between the two variables.

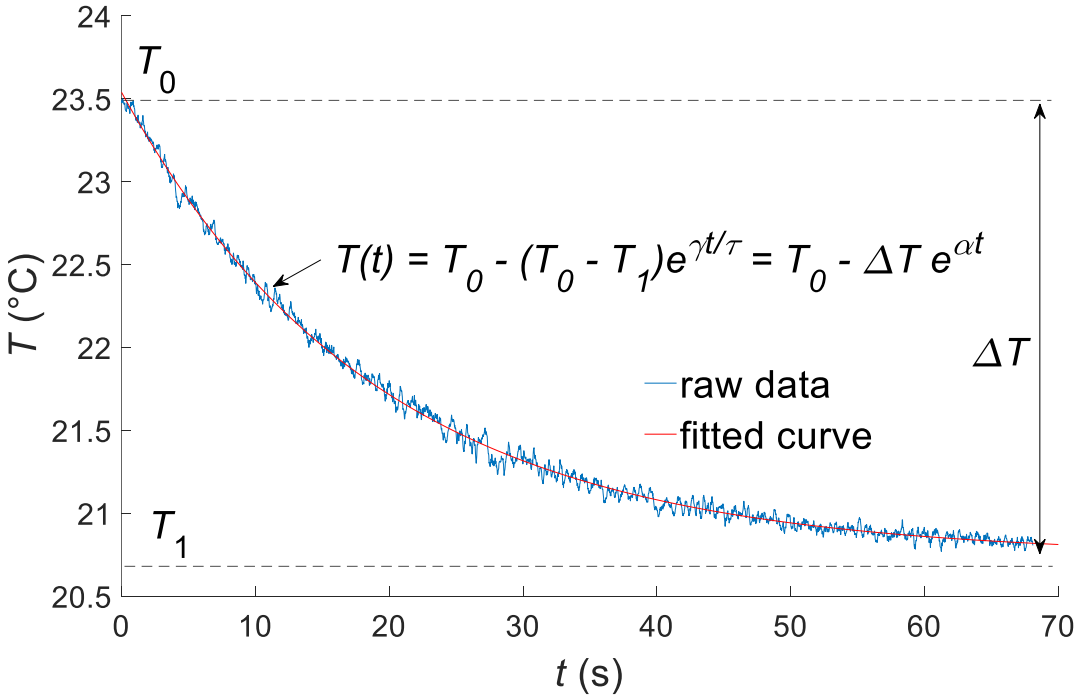

Figure 4.1: *Experimental data for a temperature-time curve and its corresponding fit*

In the first experiment the influence of the LTR height above the clamp on the cooling performance was investigated. Results are displayed in figure 4.2.

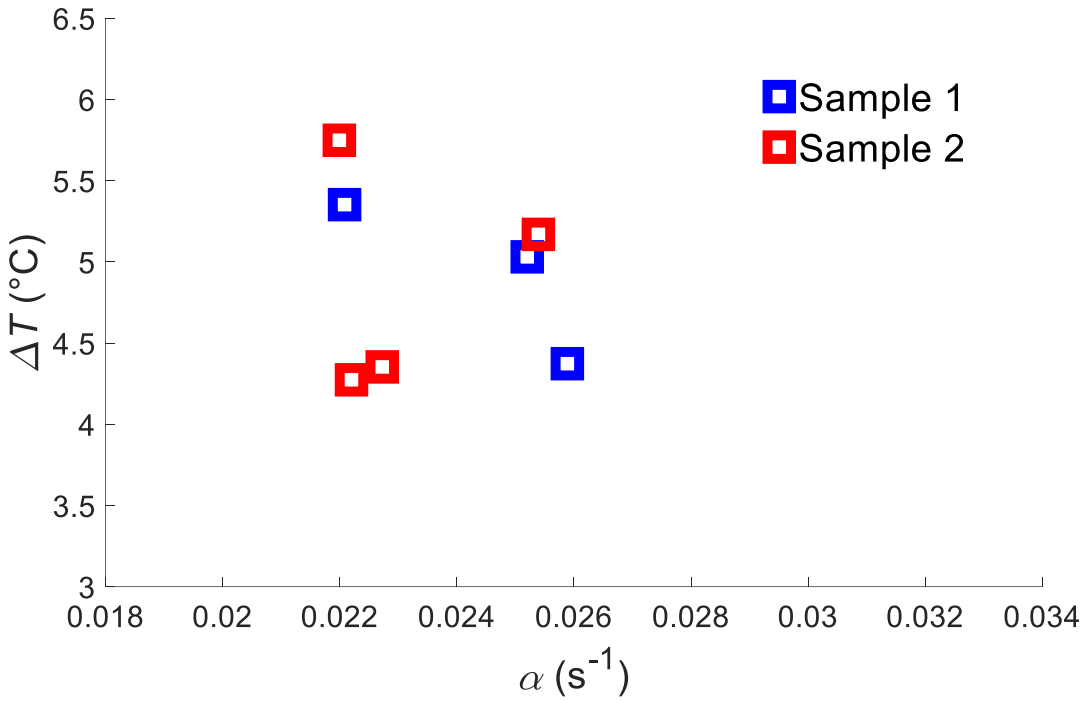

Figure 4.2: *Performance data of Sample 1 for different reservoir heights*

The best performance is achieved with the highest cylinder position. This outcome was expected. By elevating the cylinder above the clamp, a pre-stretch is applied to the elastomer membrane which leads to a strong thermal contact between membrane and LTR. Moreover, contact is established at an earlier time within the actuation cycle because the snap-back leads to instant contact with the LTR. In the case of 0 mm height, the LTR position is so low that the snap-back movement of the membrane is not sufficient to establish contact immediately. In theory, the lower LTR position would allow to reach a higher temperature difference because the membrane can fully relax after inflation. The delayed contact between membrane and LTR due to the slower deflation process explains why that is not the case.

Two brands of rubber membranes were tested as refrigerants (see Table 3.1). In order to determine the better one, both were investigated for performance and lifetime during actuation. Figure 4.3 shows the performance data of Sample 1 and Sample 2 for an actuation frequency of 0.8 Hz. Both have about the same thickness and are used representatively to compare the brands.

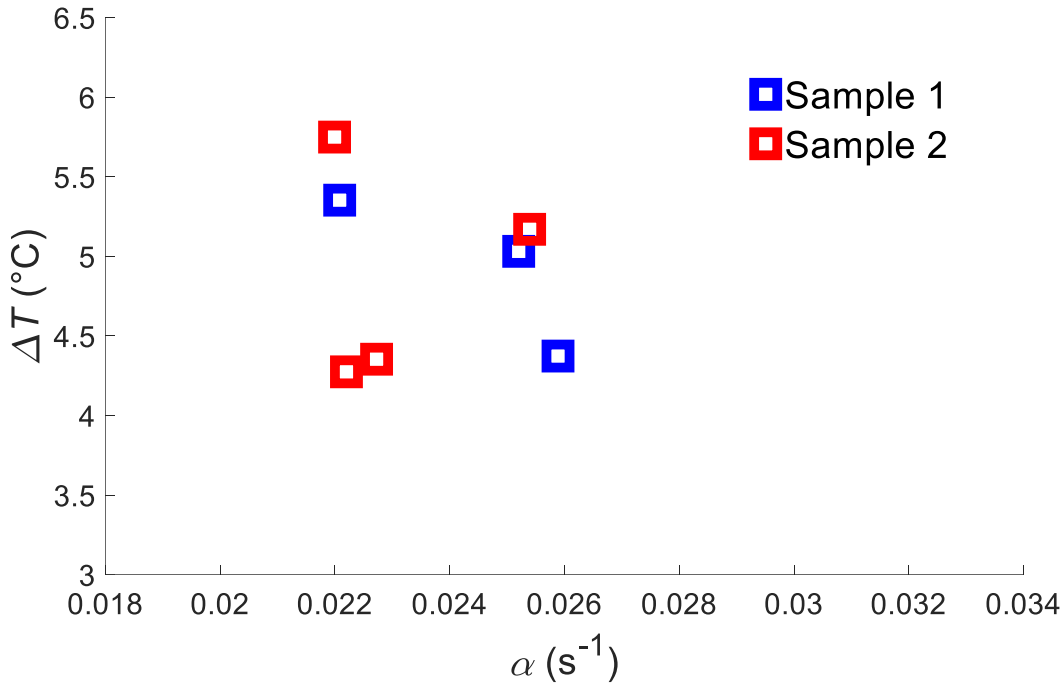

Figure 4.3: *Performance data for Sample 1 & 2*

The results show that both samples are equivalent in terms of temperature difference and decay constant, meaning, that the same cooling performance can be achieved. Next, I tested the membranes for their lifetime until fatigue. It is important to know this parameter, because the time until fatigue is the limiting operating time of the cooling device. Especially for high actuation frequencies the lifetime can be too short to reach the full cooling potential of the device. Therefore the sample with the highest mechanic stability has to be determined. A constant actuation of 0.8 Hz was applied. Every actuation cycle includes a full inflation of the membrane, where the snap-through instability is passed. Figure 4.4 shows the result for the lifetime of the membranes.

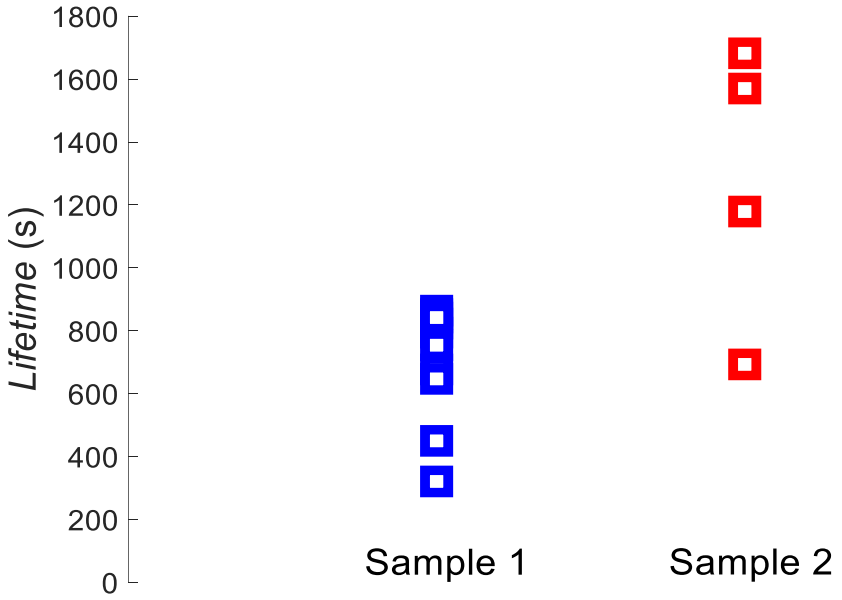

Figure 4.4: *Lifetime under actuation for Sample 1 & 2*

The lifetime of Sample 2 turns out to be far higher than for Sample 1. The reason for that is hard to determine. It is either due to a different material mixture or because of a more refined production process. At the end of a membrane life cycle one can observe spots of strong local thinning on the inflated membranes. Ultimately, these spots are the source of membrane failure and I assume that they are caused by defects introduced by production errors. The data show a high variation of the lifetimes for both samples. The statistical nature of defects gives a good explanation for that.

As a result of these preceding measurements, Samples 2-4 (same brand) were chosen for all further experiments because of their superior mechanical qualities. In a next step, I was interested in the dependence of the actuation frequency on the lifetime of the membranes in order to proof their suitability for measurements at high actuation frequencies. Figure 4.5 shows the lifetime distribution for Sample 2 for three different actuation frequencies. The data for 0.8 Hz are identical to that of figure 4.4.

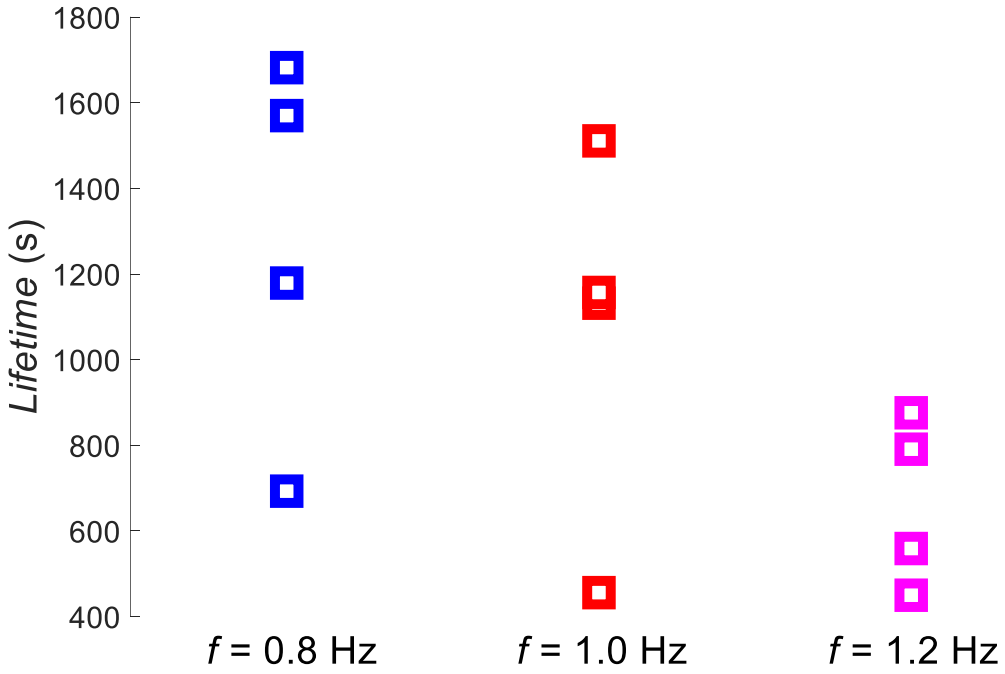

Figure 4.5: *Lifetimes for different actuation frequencies of Sample 2*

In the following experiments I investigated the influence of the clamp aperture on the cooling performance. The aperture is one of the key parameters that can be varied in the experiment. The size of the aperture determines the maximum strain achievable and also influences the amount of pressure required to trigger the snap-through instability. In order to optimize the device it is necessary to characterize how performance depends on these parameters. Three types of apertures were used, 30 mm, 35 mm and 40 mm. All measurements were performed at the same actuation frequency of 1 Hz. Two different membranes were examined, Sample 3 and Sample 4. Results are displayed in figure 4.6.

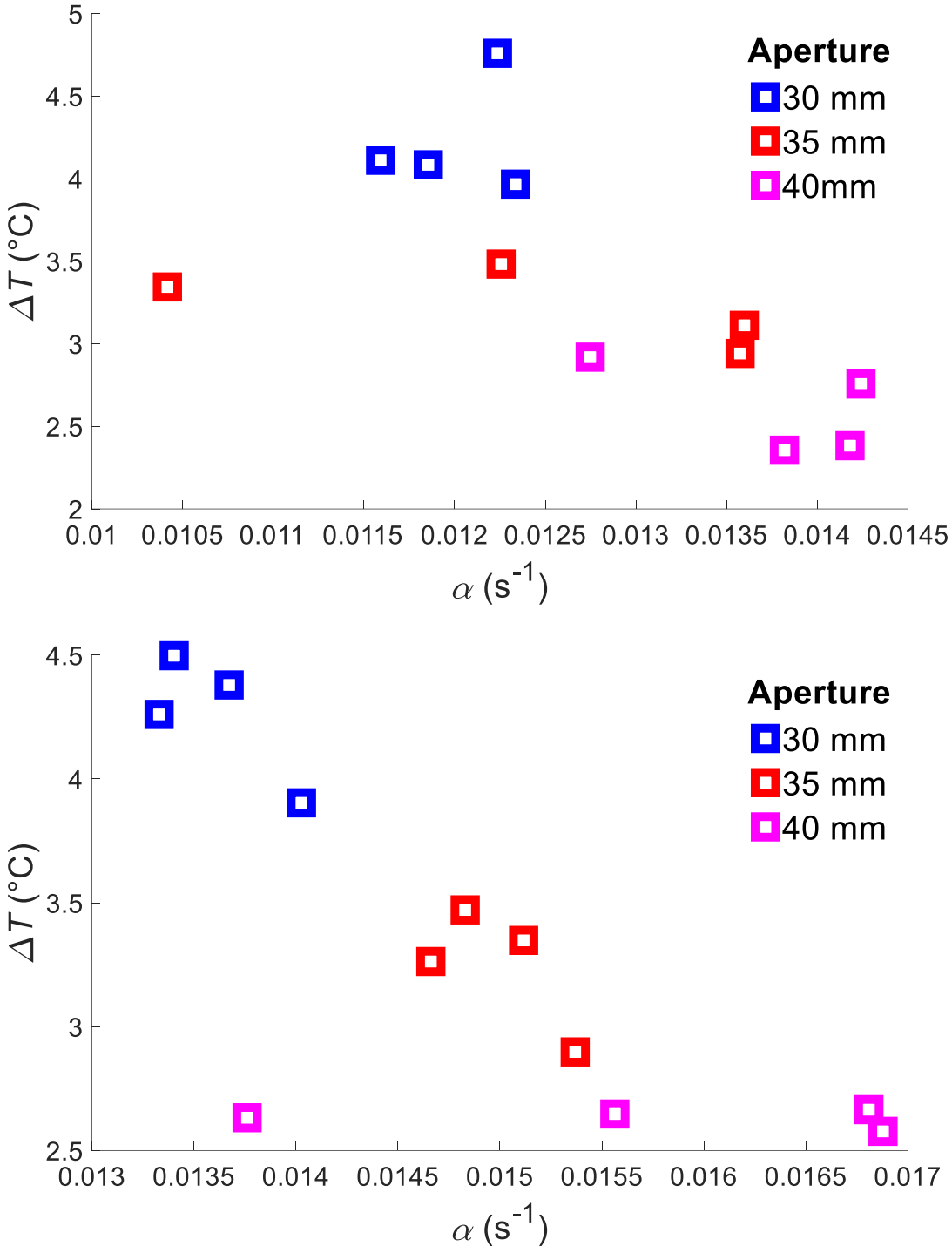

Figure 4.6: *Performance data for different apertures of Sample 4 (top) and Sample 3 (bottom)*

Unfortunately, the variation of the results for a given aperture size is too high to draw a statistically clean conclusion. Nevertheless, there is a trend visible which coincides with the expected result. The small aperture exhibits a high temperature difference, but a low decay constant. In contrast, the large aperture causes a low temperature difference, but a high decay constant. This behavior can be explained by the fact that the overall strain applied to the membrane in the smaller aperture is higher because the membrane is inflated to the same balloon volume for every aperture size. The degree of strain is proportional to the maximum temperature difference achievable (see theory

section). On the other hand, the decay constant is a measure of cooling power defined by the amount of heat transported per time. The amount of heat the membrane can transport per cycle is proportional to the heat capacity. Since the stretch of the membrane for the large aperture is lower, the membrane is thicker in the inflated state and can therefore take up more heat than in the case of the small aperture.

Coefficient of Performance and Specific Power

In order to compute the COP of the cooling device, the work required for one actuation cycle has to be measured. The method used to acquire the p-V-diagram is described in detail in the experimental section. In a first step, the accuracy of the experimental method was evaluated. Due to the mounted HTR, against which the balloon is pressed after inflation, the maximum volume during each cycle has an artificial limit. The maximum volume is determined with graphical methods to be 128 cm^3. Figure 4.7 shows a volume-time curve for one actuation cycle of 1 Hz of a Sample 3 membrane. At the beginning the volume is zero. When pressure is enhanced, the volume undergoes a flat increase until at ~0.2 s the snap-through instability leads to a quasi-instant jump in the volume curve. The device is constructed in a way that the snap leads to direct contact with the heat-sink cylinder, therefore the maximum volume is reached instantly.

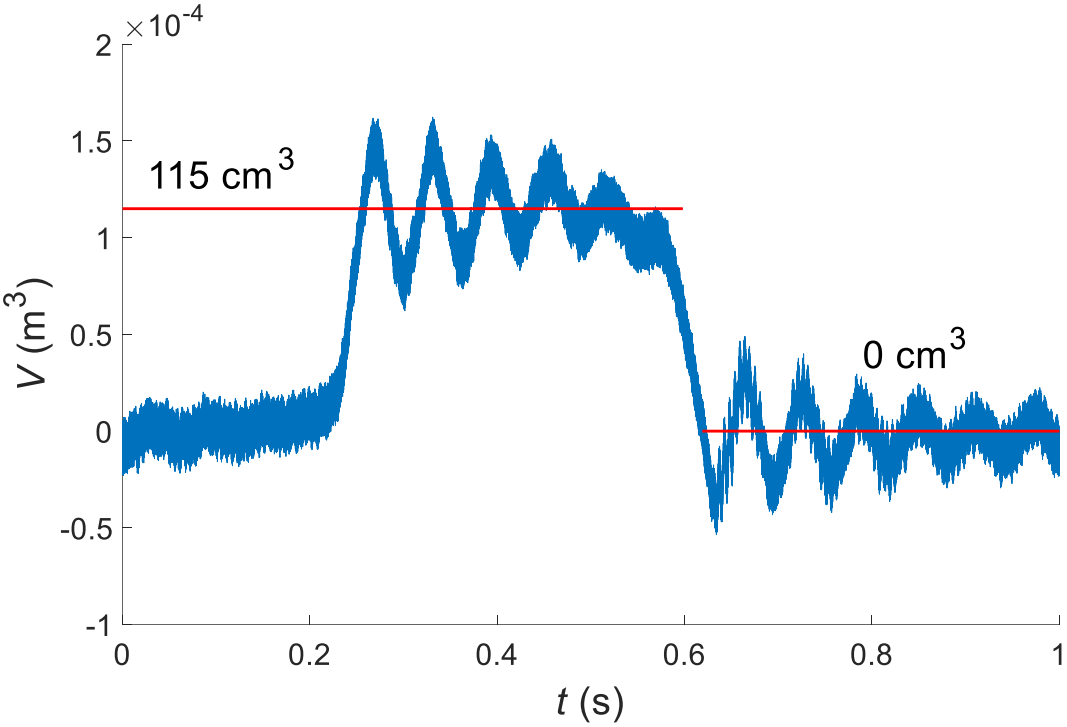

Figure 4.7: *Volume-time curve for one actuation period with mounted HTR*

A problem arises in the interpretation of the data when looking at the oscillations that occur directly after the snap-through and the snap-back of the membrane. The rapid relaxation of the membrane onto the HTR and the LTR superimposes an exponentially decaying wave of ~16 Hz over the static pressure signal. This oscillation originates from the tube connecting the cylindrical hood with the 300 L volume reservoir, which forms an open cavity resonator. Inserting the tube length into the standard acoustic formulas yields a theoretical value of about 16 Hz for the resonance frequency. The fact that the oscillation after the snap back has its mean at zero and that the asymptotic of the exponential decay converges towards zero are strong indicators that the true value can be found at the mean of the oscillation. When computing the mean of the oscillation after the snap-through, one

finds a volume of 115 cm^3 which coincides quite precisely with the graphically computed value. Therefore it can be concluded that the method for volume determination yields accurate results.

In order to determine the p-V-diagram, the p(t) and the V(t) curve are plotted. Unfortunately, the acoustic oscillations in the volume signal introduce high uncertainties into the central area of the diagram. This makes it impossible to compute a reliable value for the mechanic energy per cycle. As a solution, I removed the HTR from the device and measured the p-V-diagram without it. This strongly reduced the oscillations since there is no more impact after the snap-through. When the membrane is inflated in this modified setup with the same rate of air inflow as before, the maximum balloon volume strongly exceeds the limit value given by the mounted HTR. Therefore, in order to get a p-V-diagram with the same maximum volume, the air inflow has to be reduced. In theory that should not pose a problem since a p-V-diagram has to be parameter-independent. To confirm this, p-V-diagrams with the same membrane at three different actuation frequencies (0.5 Hz, 1 Hz, 2 Hz) were measured, which is equivalent to using different air inflows. All measurements were adjusted to yield the same maximum volume of 150 cm^3. The result shows that the energy per cycle for all three cases is identical (0.083, 0.083, 0.083 J), and therefore independent of the air inflow.

Finally, the time dependence of the energy per cycle was examined. The elastomer membrane material might change its mechanical properties during its lifetime under actuation. This might change the resulting energy per cycle depending on the moment of measurement. Three p-V-diagrams of Sample 3 & 4 at an aperture of 40 mm and a frequency of 1 Hz were acquired at three different points in time. The measurements were taken during constant periodic actuation at 30 s, 120 s, 240 s and 70 s, 200 s, 470 s respectively. Evaluation of the energies per cycle yields little to no differences (Sample 3: 0.088, 0.08, 0.076 J; Sample 4: 0.05, 0.05, 0.05 J). Therefore, the specific moment of data acquisition can be regarded as irrelevant.

Figure 4.8 shows an example of the final result for Sample 3 with an aperture of 40 mm. Measurements were performed for all membrane thicknesses and apertures (see Table 4.1). The upper two graphs show the p(t) and V(t) curves and the lower graph shows the resulting p-V-diagram. Only the part of the data relevant for computing the energy per cycle is displayed. The upper and lower flank of the p-V-diagram are numerically fitted with a polynomial of first and second degree respectively. The energy per cycle is computed by subsequent integration with boundaries from zero to the point of intersection of the fitted polynomials.

Table 4.1: *Energy per cycle (J)*

	30 mm Aperture	40 mm Aperture
Sample 2	-	0.14
Sample 3	0.12	0.07
Sample 4	0.08	0.05

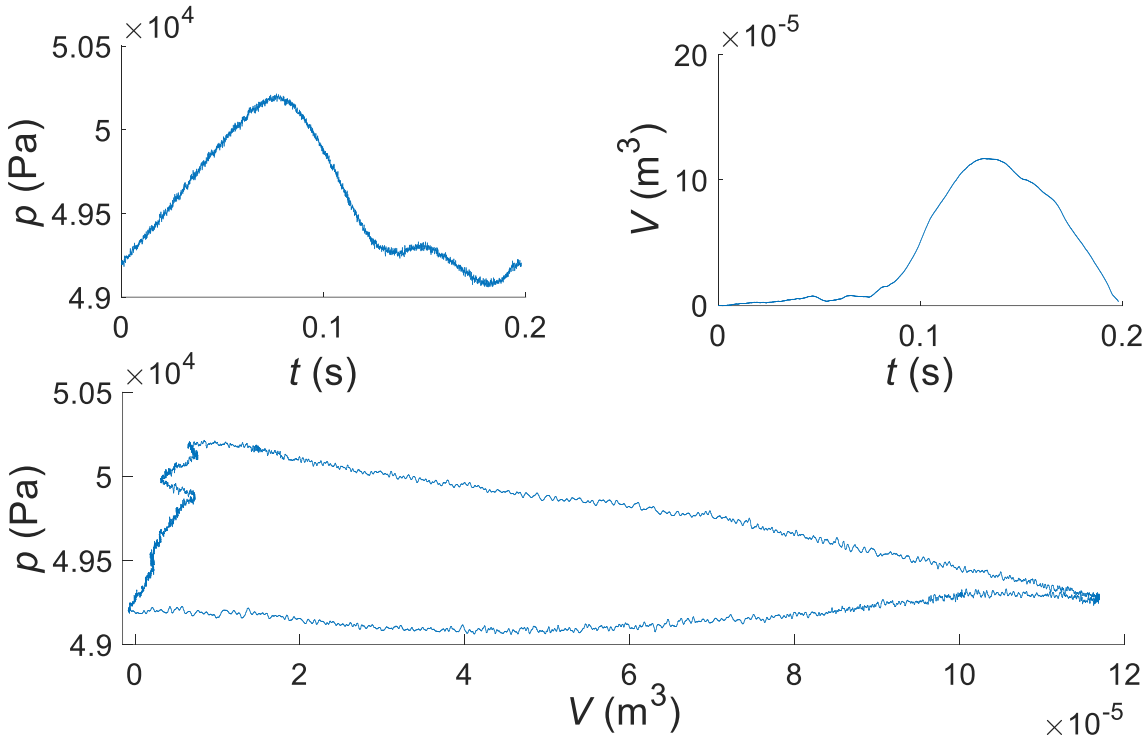

Figure 4.8: *Pressure-time curve (top left), volume-time curve (top right) and p-V-diagram (bottom) for one actuation cycle*

In order to compute the COP one needs to determine the heat transport achieved by the device. Figure 4.9 shows a measured temperature-time curve. The upper graphic displays the whole cooling cycle until reaching the minimum temperature, the area marked by the red rectangle is magnified and displayed in the lower graphic. This onset of the cooling process is the key data for determining the COP. The magnified graph shows that the temperature decay is a stepwise process. Every subsequent contact of the elastomer membrane with the reservoir leads to a steep cooling step followed by a flat plateau when the membrane has no contact. When the temperature approaches its minimum value, the net cooling effect after every cycle, i.e. the net transported heat, vanishes. This results in a COP approaching zero. The COP progresses from its maximum value at the beginning of the process to zero when equilibrium is reached. To provide a meaningful classification of the cooling performance it thus is reasonable to use the maximum COP as a standard. First, the data are fitted with an asymptotic exponential model, then the performance parameters, maximum temperature difference and decay constant, are extracted (for results see figure 4.10). The maximum heat transfer per cycle is determined by evaluating the temperature difference in the exponential model in the interval from 0 s to the length of the first actuation period. This value is then multiplied with the heat capacity of the LTR to get the transported heat per period. To compute the COP, the maximum heat transfer per cycle is divided by the mechanical actuation energy per cycle. Results for the COP with actuation frequencies of 0.5 Hz and 1 Hz are displayed in Tables 4.2 & 4.3.

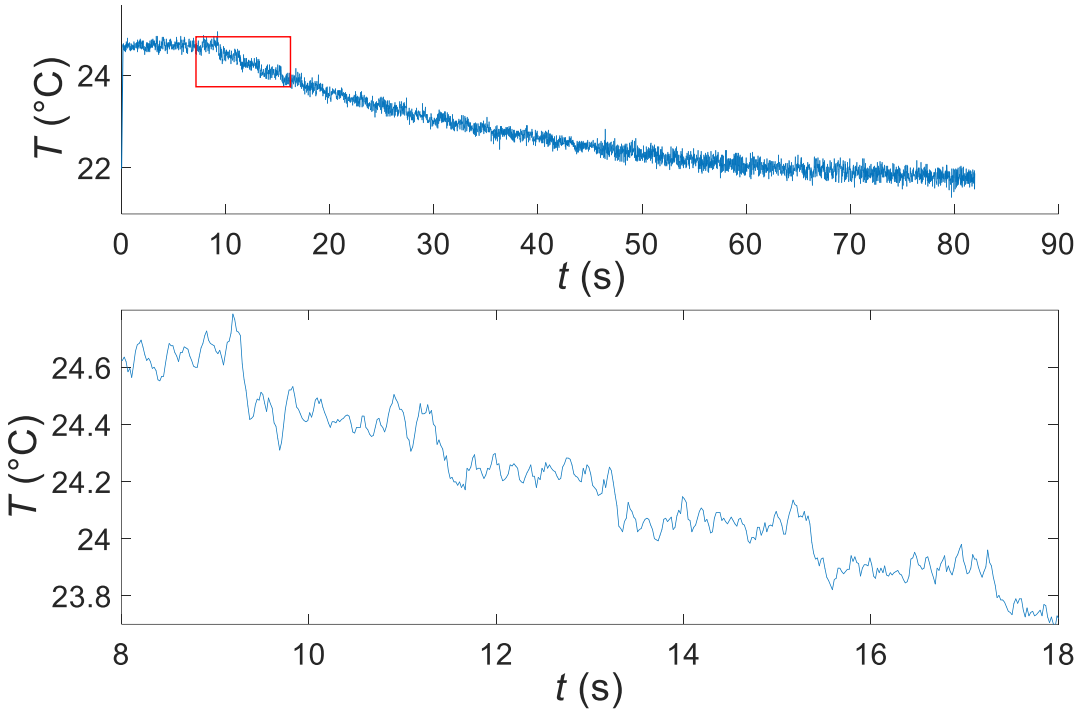

Figure 4.9: *Temperature-time curve over the whole cooling range (top) and magnified image of the onset of the cooling process (bottom)*

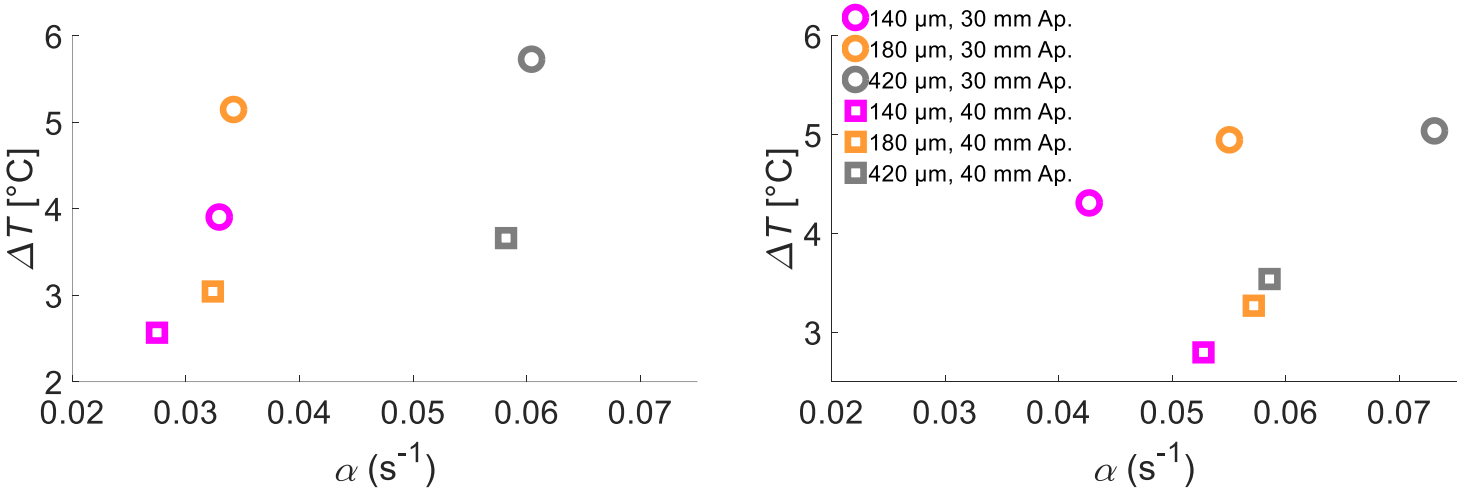

Figure 4.10: *Performance data of Samples 2-4 at 0.5 Hz (left) and 1 Hz (right)*

Table 4.2: *COP of Samples 2-4 at an actuation frequency of 0.5 Hz*

	30 mm Aperture	40 mm Aperture
Sample 2	-	3.8
Sample 3	3.6	3.5
Sample 4	3.9	3.8

Table 4.3: *COP of Samples 2-4 at an actuation frequency of 1 Hz*

	30 mm Aperture	40 mm Aperture
Sample 2	-	1.9
Sample 3	2.8	3.3
Sample 4	2.8	3.5

The specific power is defined as the power per unit mass of cooling agent and given in (W/g). First the power has to be determined. The transported heat per cycle used for calculating the COP has the unit of power, since the cycle period has the unit of time. It can be directly used to compute the specific power by normalizing it to unit time. This is done by dividing the transported heat per cycle by the length of the cycle period.

Secondly, the mass of the elastomer membrane directly in touch with the LTR has to be determined. The weight of the initial membrane sheet is multiplied with a geometric exclusion factor which accounts for the fact that only a fraction of the area of the sheet is in direct contact with the LTR. This factor contains corrections for the difference in area of the sheet and the LTR, as well as for the membrane thinning caused by the pre-stretch due to the elevated LTR cylinder. The correction factor amounts to 0.33 for the 30 mm aperture and to 0.59 for the 40 mm aperture. Table 4.4 shows the values of the effective masses of the elastomer membranes in contact with the LTR. Table 4.5 shows the results for the specific power.

Table 4.4: *Effective membrane mass (g) of Samples 2-4*

	30 mm Aperture	40 mm Aperture
Sample 2	0.26	0.47
Sample 3	0.11	0.2
Sample 4	0.08	0.15

Table 4.5: *Specific Power (W/g) of Samples 2-4*

	30 mm Aperture	40 mm Aperture
Sample 2	1.7	0.6
Sample 3	3.0	1.2
Sample 4	2.8	1.3

Dielectric Elastomer Actuator

A proof of concept DEA system was realized, which is able to provide the pressure difference necessary for actuation with electric energy (see experimental section). Up to five DEAs are operated simultaneously. The required power is delivered by a high-voltage supply coupled to a signal generator which modulates the output to a sine-wave. To start the operation, a constant offset pressure is applied to the pressure vessel to inflate both the elastomer membrane and the DEAs. When a voltage is applied to the DEA, the VHB membranes sandwiched between the carbon grease electrodes thin down due to electrostriction. As a result the DEA increases its volume and, because the volume inside the pressure vessel has to remain constant, the elastomer membrane balloon decreases its volume. If the applied voltage is high enough, the achieved pressure difference can periodically trigger the snap through instability. The number of DEAs used in the system determines the maximum volume change achievable, while the number of VHB layers in each individual DEA determines the maximum pressure difference achievable. Not only does the number of layers decide whether the system is strong enough to provide sufficient pressure, it also determines the elastic modulus of the DEA. In order to achieve a comparable degree of inflation of both the DEAs and the elastomer membrane, the system has to be carefully balanced. The modulus of the elastomer membrane always remains fairly constant, while the modulus of the DEA can be modified. One way to do so is by letting the DEA age. As a result, the silicon oil in the carbon grease electrode will diffuse into the VHB layers and lower the modulus. Also, the DEA can be “trained” by periodic inflation to very high volumes for a short time. This process leads to molecular shifts within the VHB which lower the required pressure for inflation. A balanced inflation is crucial for the system to work. A DEA with a low modulus will overinflate and become prone to dielectric or mechanic failure. A high modulus DEA will only inflate to a small degree. As a consequence the VHB-membrane thickness will remain too high to achieve the field strengths required to produce the necessary volume difference during actuation. Actuation of the elastomer membrane was achieved with Sample 4 at an aperture of 40 mm and actuation frequencies of 1-3 Hz, and at an aperture of 35 mm with 1 Hz. Sample 3 was actuated at an aperture of 40 mm with frequencies of 1-2 Hz. It is remarkable that the DEA system allows for higher actuating frequencies than actuation with pressurized air.

The temperature drop achieved when actuating the system with DEAs is slightly lower than for actuation with pressurized air. I assume that is due to the lower pressure during contact with the HTR which leads to a less effective heat transfer. The power consumed by the DEA system is computed by integrating the product of voltage and current over one period of actuation. Figure 4.11 shows an example for the graphs of these parameters. The upper two graphs show the U(t) and I(t) curves and the lower graph shows the resulting power P(t). The current has a phase shift relative to the voltage, leading to an asymmetric shape of the power graph. This results in quite significant energy consumption of the DEA in the range of 0.3-0.7 Watts per cycle, yielding an efficiency orders of magnitude lower than what is theoretically possible. However, it should be mentioned that this problem has a high potential of improvement by modifying the system with a suitable electrical circuit able to neutralize the phase shift of the current introduced by the DEAs.

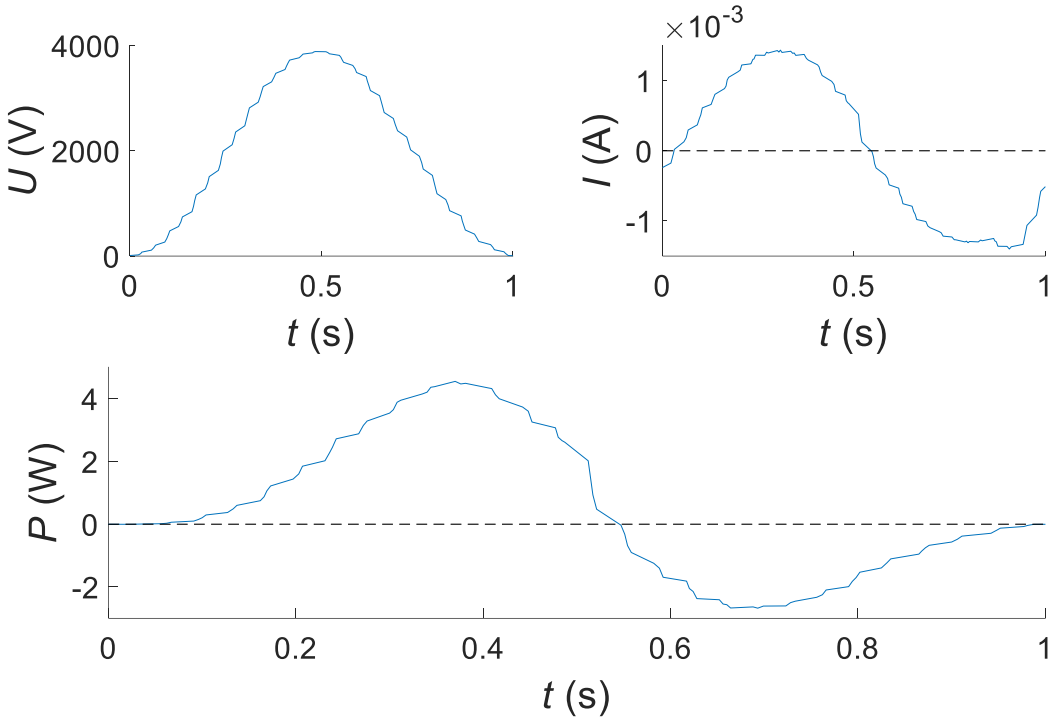

Figure 4.11: *Voltage-time curve (top left), current-time curve (top right) and power-time curve (bottom) of the DEA system.*

Conclusion

In this thesis a novel refrigeration system based on the elastocaloric effect of rubber is demonstrated. The results show the feasibility of rubber as a cooling agent, when the material is stretched and relaxed periodically. Both, the stretching and the relaxation are achieved via inflation of the rubber membrane into a balloon. The growing balloon reaches a snap-through instability which causes a rapid expansion and an adiabatic temperature change of the rubber membrane. Temperature differences of up to 5 °C are achieved under constant operation with the experimental system. The rubber balloon operates between two customized heat reservoirs which assist fast thermal equilibration of the membrane and maximize the efficiency, expressed by the coefficient of performance (COP). A maximum COP of ~4 has been reached by the first prototype. This value is comparable to state-of-the-art refrigeration systems.

The system developed and investigated in this thesis is driven with pressurized air. With the goal of becoming independent of pressurized air, an electrostatic actuation system based on dielectric elastomer actuators (DEA) was developed. The DEAs transfer the refrigeration system into a stand-alone device which is independent of an external pressure supply. The achieved results indicate a promising new class of refrigeration systems with high potential for further improvement.

Outlook

The results presented in the previous section demonstrate the extraordinary cooling capability of rubber. However, as promising as the results may be, there remains a lot of room for improvement. The elastomer membrane can deliver a maximum temperature difference of 12 °C when fully extended. Therefore a lower cooling temperature could be achieved by increasing the volume of inflation. Such a temperature drop would make the technology feasible for food refrigeration and air conditioning. Alternatively, the development of a stacked cooling system should be considered using several elastomer membranes connected in series to achieve a high cumulative temperature drop.

A possible pathway to achieve an even higher temperature difference of 20 °C was discovered by Tiller [26]. He showed that the latent heat of strain-induced rubber crystallization can be used to enhance the temperature drop upon relaxation beyond the elastocaloric cooling capability of the material. The additional temperature difference is caused by a phase transition, therefore the amount of work required for actuation remains the same as before. This opens up a perspective towards a leap in efficiency of elastomer-based cooling systems.

The optimization of experimental parameters holds a lot of potential for an improvement of efficiency. A thorough examination towards the ideal duration of inflation and deflation periods needs to be carried out. Since membrane thicknesses vary depending on the state of inflation, it is likely that the time required to cool down the inflated membrane is shorter than to heat up the deflated membrane. Also, constant operation of the cooling process over an extended period of time leads to a significant heating of the HTR. For maximum performance, the HTR should be coupled to an additional reservoir (e.g. water) to keep it at the initial temperature.

There remain two major challenges for this technology to become suitable for commercial use:

First, the major limiting factor is the short lifetime of the elastomer membrane. The maximum lifetime of about 30 minutes is many orders of magnitude shorter than a typical refrigerator lifetime of about 10 years. Advances in material science are necessary for further development in this area.

Secondly, the high energy consumption of the DEA needs to be reduced to the minimum required for the actuation of the elastomer membrane. A possible solution is the introduction of inductive elements into the electric circuit. Together with the DEAs as capacitance they would form an LC-resonator allowing for energy recovery. Furthermore, the lifetime of the DEAs has to be increased. Although it is significantly higher than for the elastomer membrane, it is by far not sufficient for commercial operation. In order to increase mechanic long-term stability, the carbon-grease electrode has to be exchanged for a non-fluid material (as proposed in Supplements) because the silicon oil in the carbon grease lowers the mechanic stability of the VHB dielectric. However, there remains the problem that electric breakthrough will eventually destroy the DEA. A possible approach to solving this problem is given by Keplinger [27] who developed DEAs which are immune to electric breakthrough. However, it should be noted that the design proposed in the paper would require heavy modification to allow its use in my cooling system.

Supplements

Carbon Black Mixes

The carbon grease electrode used in the experiments is messy to handle since it stains everything it touches. To make matters worse, it is very difficult to clean off of any surface. Therefore attempts were made to develop a flexible carbon black electrode based on polydimethylsiloxane (PDMS). Such an electrode could be readily touched without causing any stains. By tackling this problem one faces multiple challenges. As mentioned in the theory section, the modulus of the electrode has to be lower than the actuating material to avoid reduced DEA performance. Since the modulus of PDMS is generally higher than for VHB, very thin sheets have to be produced to overcome this problem. However, thinner sheets are more prone to production defects and hence, to mechanic failure. This is especially problematic because for the use in a DEA they need to withstand very high strains in the order of 3 (3x3 linear strain). This value is close to the maximum extensibility of PDMS.

Another problem is the electric conductivity. Carbon black is used to make the membranes electrically conductive and has a directly negative effect on their mechanical properties. By increasing the ratio of carbon black in the membrane, the maximum extensibility and tensile strength worsen significantly. At the same time, more carbon black improves the conductivity of the material. The electrical resistivity should not exceed a value of about 200 kΩ in order to be of use in a DEA. One needs to consider that by inflating the membrane the area expands and the thickness is reduced. This causes a further increase of the overall resistivity, though the effect is not as strong as one would expect from a geometric point of view. I suppose that improved contact between carbon black particles due to the compressive stress acting normal to the plane of expansion mitigates the decrease in conductivity. However, this effect was not further examined.

Membrane Production

A glass plate covered with 6 µm polyethylene-terephtalate (PET) foil served as a substrate for membrane production. To enable a wrinkle-free coverage, the contact between glass plate and foil is improved with a few drops of isopropanol. After applying the foil, its ends are folded around the edges of the plate and fixed with glue. Finally the surface of the foil is flattened by gently stroking it from the center outwards with a dough scraper. Before pouring the PDMS-mixture on the substrate, the foil is coated with a release agent (R&G GmbH, Waldenbuch, Germany) to ensure tear-free separation after the polymerization process.

Every mixture produced consists of the same basic ingredients:

- Platinum-cured two-component PDMS with different degrees of shore hardness to choose from (Ecoflex 10, 30, 35 fast, 50)
- Carbon black powder (Black Pearls 2000, XPB545)
- Organic solvent (isopropanol, isooctane).

The mixing procedure can be broken down into four general steps, specific parameters vary depending on the recipe used (see below):

- The first step serves to disperse the carbon black particles. The Ecoflex is not yet added during this step because the extended mixing process leads to significant heat generation which would cause the elastomer to polymerize prematurely. The carbon black and the organic solvent are poured into a vessel and five steel balls (4-6 mm diameter) are added to enhance homogenization. The ingredients are mixed in a speed mixer at 2000 rpm for 10 minutes.

- For the second mixing step, Ecoflex is added to the vessel and blended in under vacuum. This serves to free the mixture of enclosed air which would otherwise weaken the mechanical properties of the material.
- The steel balls are removed from the vessel and the mixture is poured on the PET-covered glass plate and flattened with a ZUA-2000 applicator (Zehntner, Sissach, Switzerland) at a gap height of 1500 µm. The flattening step must only be carried out once. Repeated flattening causes an irregular surface and should be avoided.
- The membrane is cured in a ventilated oven. Ventilation is important to allow the organic solvent to evaporate out of the elastomer. If circulation is insufficient, the polymerization will be inhibited.

Four samples with different compositions and thicknesses were produced and tested for conductivity and tensile strength. Table 7.1 shows the mass composition of each sample and Table 7.2 outlines the steps of the mixing and curing procedure. It should be noted that the carbon black used in Sample 4 has an inhibiting effect on the polymerization of Ecoflex except for type 35. The carbon black is treated with a surfactant which I suspect to be responsible for deactivating the platinum catalyst. Ecoflex 35 contains an exceptionally high amount of catalyst and is therefore able to trigger polymerization despite the counteracting effect of the carbon black. Table 7.3 shows the electrical and mechanical properties of the samples. The thicknesses of the samples are different because in my setup they were not a controllable parameter. The membrane thickness depends on the gauge height, the gauge speed and the mixture viscosity. The mixture viscosity is different for every sample due to different compositions and the gauge speed varies because flattening is done manually. The electrical conductivity of a membrane depends on whether it is measured on the top side or the rear side. It turns out that conductivity on the rear side of the membrane (the side in contact with the PET-foil) is one order of magnitude higher than on the top side. This might be caused by sedimentation of the carbon black during the polymerization process or due to a surface effect. The resistance was measured at a probe distance of 10 mm and of 70 mm respectively, a mean value of three measurements was determined for every sample. In case of Sample 4 the variation of the measured values was quite high. I observed that the Ecoflex 35 had already started to polymerize during the mixing process which might have resulted in inhomogeneous mixing.

Figure 5.1 displays the force-strain curve of the samples 1-4 together with a fifth sample of pure Ecoflex 50 (thickness: 700 µm), serving as a benchmark for the carbon black mixtures. The ordinate displays the force measured by the force-gauge on one of the clamps of the radial stretcher. The unsteadiness of the graph in figure 5.1 is the result of a defect in the measuring instrument and not due to a material property.

Table 7.1: *Sample type and mass composition*

Sample Name	Carbon Black Type	Carbon Black Mass (%)	Ecoflex Type	Ecoflex Mass (%)	Solvent Type	Solvent Mass (%)
Sample 1	CB 545	4	10	48	Isopropanol	48
Sample 2	CB 545	4	50	48	Isopropanol	48
Sample 3	CB 545	3	10	48.5	Isopropanol	48.5
Sample 4	Black Pearls	2.4	35	48.8	Isooctane	48.8

Table 7.2: *Mixing procedure*

Sample Name	Mixing Speed (rpm)	Mixing Pressure 1 (mbar)	Mixing Time 1 (s)	Mixing Pressure 2 (mbar)	Mixing Time 2 (s)	Curing Temperature (°C)	Curing Time (h)
Sample 1	2000	90	120	50	60	70	96
Sample 2	2000	90	120	50	60	70	96
Sample 3	2000	90	120	50	60	70	96
Sample 4	1200	500	30	90	90	20	0.16

Table 7.3: *Sample properties*

Sample Name	Thickness (µm)	Resistivity at 10 mm distance (kΩ)	Resistivity at 70 mm distance (kΩ)	Maximum Extensibility (%)	Tensile Strength (?)
Sample 1	470	14.4	18.9	366	
Sample 2	450	15.8	23	490	
Sample 3	200	140	143	350	
Sample 4	550	226	296	900	

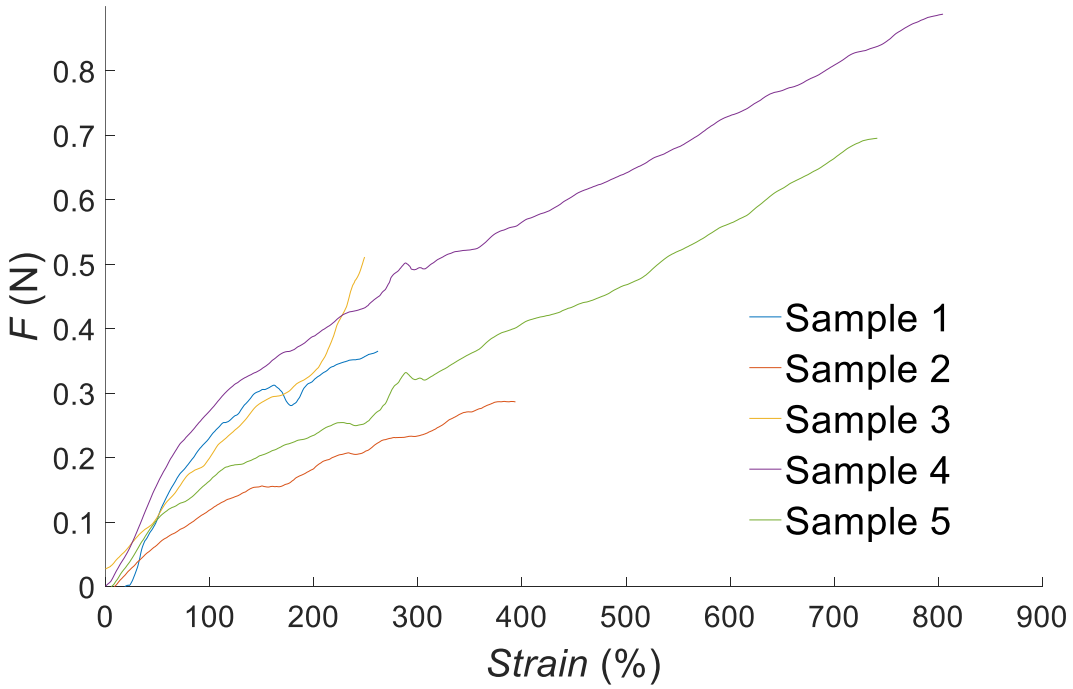

Figure 7.1: *Force-strain curve for Samples 1-4 and an Ecoflex 50 membrane.*

References

1. *The Future of Cooling*. 2018, OECD/IEA.
2. Takeuchi, I. and K. Sandeman, *Solid-state cooling with caloric materials.* Physics today, 2015. **68**(12): p. 48.
3. Gough, J., *A description of a property of Caoutchouc, or Indian rubber.* Memories of the Literacy and Philosophical Society of Manchester, 1805. **1**: p. 288-295.
4. Mullen, J., G.W. Look, and J. Konkel, *Thermodynamics of a simple rubber-band heat engine.* American Journal of Physics, 1975. **43**(4): p. 349-353.
5. Joule, J.P., *V. On some thermo-dynamic properties of solids.* Philosophical Transactions of the Royal Society of London, 1859. **149**: p. 91-131.
6. Wiegand, W. and J. Snyder, *The rubber pendulum, the Joule effect, and the dynamic stress-strain curve.* Rubber Chemistry and Technology, 1935. **8**(2): p. 151-173.
7. Farris, R.J., *Rubber heat engines, analyses and theory.* Polymer Engineering & Science, 1977. **17**(10): p. 737-744.
8. Lyon, R.E., et al., *Polyurethane–urea elastomers as working substances in rubber heat engines.* Journal of applied polymer science, 1984. **29**(9): p. 2857-2872.
9. Guyomar, D., et al., *Elastocaloric modeling of natural rubber.* Applied Thermal Engineering, 2013. **57**(1-2): p. 33-38.
10. Gerlach, D.W. *Design concepts and development of elastomer heat engines/pumps*. in *ASME 2009 International Mechanical Engineering Congress and Exposition*. 2009. American Society of Mechanical Engineers.
11. Steinberg, I., A. Oplatka, and A. Katchalsky, *Mechanochemical engines.* Nature, 1966. **210**(5036): p. 568.
12. Hutchinson, W.D., *Manually operated elastomer heat pump.* 1970.
13. Suo, Z., *Theory of dielectric elastomers.* Acta Mechanica Solida Sinica, 2010. **23**(6): p. 549-578.
14. Meyer, K.H., *Zur Geschichte der Theorie der Kautschukelastizität. Erwiderung auf die vorangehende Mitteilung.* Helvetica Chimica Acta, 1939. **22**(1): p. 1362-1364.
15. Treloar, L.R.G., *The physics of rubber elasticity*. 1975: Oxford University Press, USA.
16. Wood, L.A. and F.L. Roth, *Stress-Temperature Relations in a Pure-Gum Vulcanizate of Natural Rubber.* Journal of Applied Physics, 1944. **15**(11): p. 781-789.
17. Anthony, R.L., R.H. Caston, and E. Guth, *Equations of state for natural and synthetic rubber-like materials. I. Unaccelerated natural soft rubber.* The Journal of Physical Chemistry, 1942. **46**(8): p. 826-840.
18. Kuhn, W., *Über die gestalt fadenförmiger moleküle in lösungen.* Kolloid-Zeitschrift, 1934. **68**(1): p. 2-15.
19. Guth, E. and H. Mark, *Zur innermolekularen, Statistik, insbesondere bei Kettenmolekiilen I.* Monatshefte für Chemie und verwandte Teile anderer Wissenschaften, 1934. **65**(1): p. 93-121.
20. Wall, F.T., *Statistical Thermodynamics of Rubber. III.* The Journal of Chemical Physics, 1943. **11**(11): p. 527-530.
21. Flory, P.J. and M. Volkenstein, *Statistical mechanics of chain molecules*. 1969, Wiley Online Library.
22. Gent, A., *A new constitutive relation for rubber.* Rubber chemistry and technology, 1996. **69**(1): p. 59-61.
23. Green, A.E., R. Shield, and R. Rivlin, *General theory of small elastic deformations superposed on finite elastic deformations*, in *Collected Papers of RS Rivlin*. 1997, Springer. p. 589-616.
24. Adkins, J.E. and R. Rivlin, *Large elastic deformations of isotropic materials IX. The deformation of thin shells.* Phil. Trans. R. Soc. Lond. A, 1952. **244**(888): p. 505-531.
25. Carslaw, H. and J. Jaeger, *Conduction of heat in solids: Oxford Science Publications*. 1959: Oxford, England.

26. Katzenberg, F., B. Heuwers, and J.C. Tiller, *Superheated rubber for cold storage.* Advanced Materials, 2011. **23**(16): p. 1909-1911.
27. Acome, E., et al., *Hydraulically amplified self-healing electrostatic actuators with muscle-like performance.* Science, 2018. **359**(6371): p. 61-65.